WILEY-VCH

Edited by Liudmil Antonov

Tautomerism

Concepts and Applications in Science and Technology

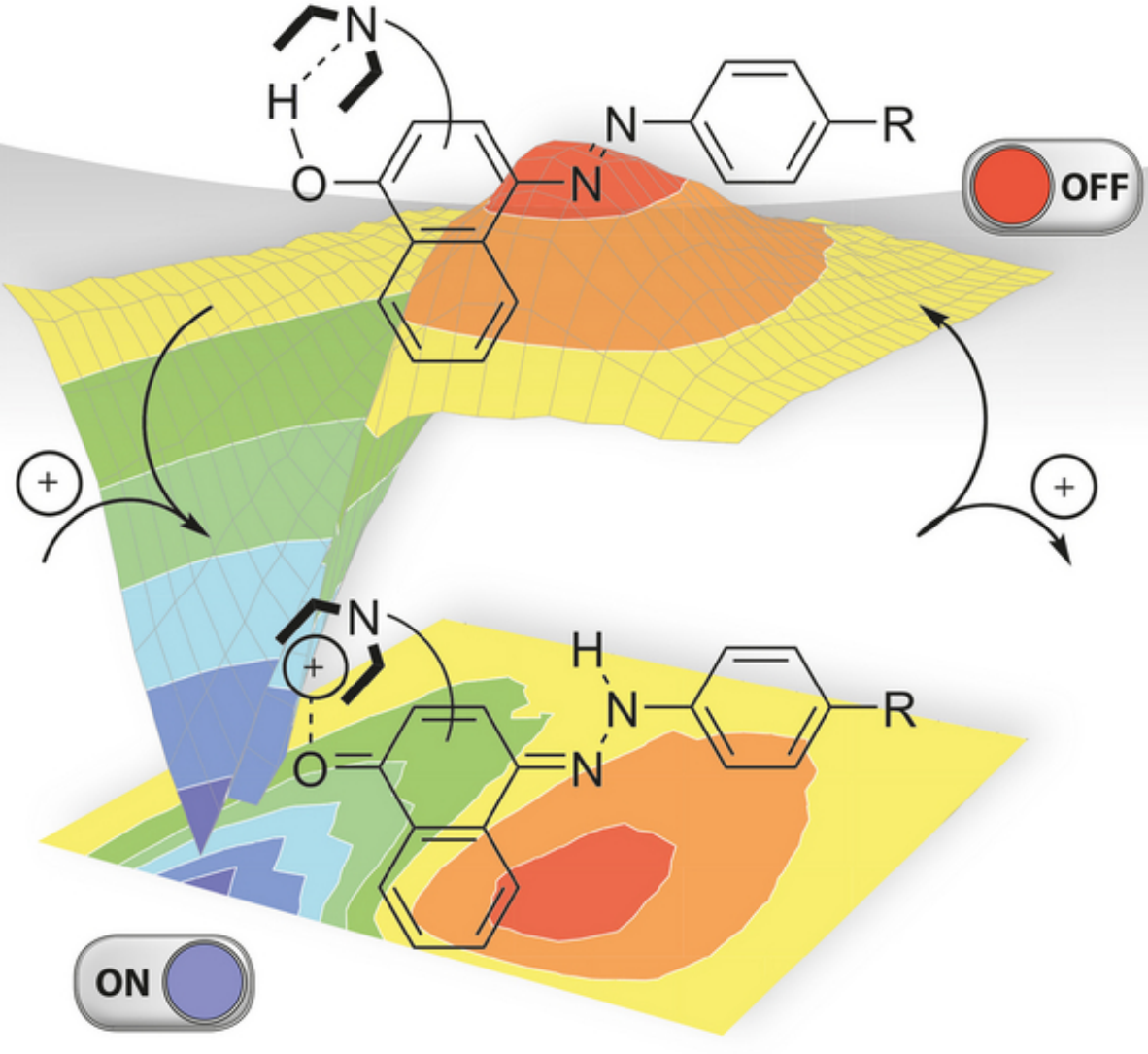

Editor

Prof. Liudmil Antonov
Bulgarian Academy of Sciences
Inst. of Organic Chemistry
Acad. G.Bonchev str., bl.9
1113 Sofia
Bulgaria

Cover The cover shows a sketch of the controlled switching in a structurally modified 4-(phenyldiazenyl)naphthalen-1-ol. The flash photolysis surface, describing the process is shown as background image.
Designed by Mihaela Antonova.

Library of Congress Card No.: applied for

British Library Cataloguing-in-Publication Data
A catalogue record for this book is available from the British Library.

Bibliographic information published by the Deutsche Nationalbibliothek
The Deutsche Nationalbibliothek lists this publication in the Deutsche Nationalbibliografie; detailed bibliographic data are available on the Internet at <http://dnb.d-nb.de>.

Print ISBN: 978-3-527-33995-2
ePDF ISBN: 978-3-527-69574-4
ePub ISBN: 978-3-527-69572-0
Mobi ISBN: 978-3-527-69573-7
oBook ISBN: 978-3-527-69571-3

Typesetting SPi Global, Chennai, India
Printing and Binding

Printed on acid-free paper

Contents

List of Contributors *XV*
Preface *XIX*

1 Tautomerism: A Historical Perspective *1*
José Elguero
1.1 Thermodynamic Aspects *2*
1.1.1 What Is Well Known *2*
1.1.2 What Needs to Be Completed *3*
1.1.3 What Is Ill Known *4*
1.2 Kinetic Aspects *5*
1.2.1 What Is Well Known *5*
1.2.2 What Needs to Be Completed *6*
1.2.3 What Is Ill Known *6*
1.3 Conclusions *6*
References *7*

2 "Triage" for Tautomers: The Choice between Experiment and Computation *11*
Peter J. Taylor and Liudmil Antonov
2.1 Introduction (Original Text Written by Peter J. Taylor) *11*
2.2 *cis*-Amides *12*
2.3 Tautomerism in Alicyclic Lactams: Six-Membered Rings *13*
2.4 Tautomerism in Alicyclic Lactams: 2-Pyrrolidinone *14*
2.5 Tautomerism in Other Five-Membered Ring Lactams *16*
2.6 Tautomeric Ratios Requiring Computation: Alicyclic β-Diketones *17*
2.7 Tautomeric Ratios Requiring Computation: "Maleic Hydrazide" *18*
2.8 Tautomer Ratios Requiring Computation: 2-Oxo Derivatives of Pyrrole, Furan, and Thiazole *20*
2.9 Tautomeric Ratios Requiring Computation: Compounds Containing Contiguous Carbonyl Groups *22*
2.10 Tautomeric Ratios Requiring Computation: Compounds Containing Contiguous π-Donors *24*

2.11 Compounds Equally Suited to Experiment or Computation: "Azapentalenes" *25*
2.12 Phenomena Susceptible to Experiment or Computation: Lone Pair Effects *29*
2.13 Conformational Effects on Aminoenone Stability: A Computational Approach *30*
2.14 Overview (Original Text Written by Peter J. Taylor) *32*
References *32*

3 Methods to Distinguish Tautomeric Cases from Static Ones *35*
Poul Erik Hansen
3.1 Introduction *35*
3.2 The Liquid State *36*
3.2.1 NMR *36*
3.2.1.1 ^{1}H NMR *36*
3.2.1.2 ^{15}N NMR *38*
3.2.1.3 ^{13}C Chemical Shifts *39*
3.2.1.4 ^{19}F NMR *41*
3.2.1.5 ^{17}O NMR *41*
3.2.2 Isotope Effects on Chemical Shifts *42*
3.2.2.1 Deuterium Isotope Effects on ^{13}C Chemical Shifts *44*
3.2.2.2 Deuterium Isotope Effects on ^{15}N Chemical Shifts *47*
3.2.2.3 Deuterium Isotope Effects on ^{17}O Chemical Shifts *47*
3.2.2.4 Isotopic Perturbation of Equilibrium *47*
3.2.2.5 Primary Isotope Effects *48*
3.2.3 Coupling Constants *51*
3.2.3.1 ^{1}J(N,H) *51*
3.2.3.2 ^{1}J(C,H) *52*
3.2.4 Multiple Equilibria *52*
3.3 UV/VIS Spectroscopy *53*
3.4 Infra Red Spectroscopy *55*
3.4.1 Ambient temperature spectra *55*
3.4.2 Matrix isolation spectra *56*
3.5 Tautomerism in the Excited State *56*
3.6 Near-Edge X-Ray *56*
3.7 Energy-Dispersive X-Ray *57*
3.8 Solid State *57*
3.8.1 NMR *57*
3.8.1.1 Isotope Effects on Chemical Shifts *58*
3.8.2 X-Ray *59*
3.9 Single Molecule Tautomerization *59*
3.10 Gas Phase *60*
3.11 Theoretical Calculations *61*
3.11.1 Energies *62*
3.11.2 NMR Chemical Shifts *62*

3.11.3 Coupling Constants *66*
3.11.4 Isotope Effects on Chemical Shifts *68*
3.11.5 Vibrational Spectra *70*
References *71*

4 Electron-Transfer-Induced Tautomerizations *75*
Thomas Bally
4.1 Introduction *75*
4.2 Methodology *76*
4.3 *O*-Alkyl Phenyl Ketones *77*
4.3.1 *O*-Methylbenzophenone *78*
4.3.2 *O*-Alkylacetophenone Derivatives *80*
4.3.3 *O*-Methylacetophenone *81*
4.3.4 7-Methyl- and 4,7-Dimethyl-1-indanone *83*
4.3.5 NADH Analogs *88*
4.3.6 Other Cases of Tautomerizations in Radical Cations *91*
4.4 Conclusions *93*
Acknowledgments *93*
References *94*

5 The Fault Line in Prototropic Tautomerism *95*
Peter J. Taylor and Liudmil Antonov
5.1 Introduction: "*N*-Type" and "*C*-Type" Tautomerism *95*
5.2 Tautomerism in Symmetrical Amidines *96*
5.3 Tautomer Ratio in Asymmetric Heteroaromatic Amidines *100*
5.4 Tautomer Ratio in the Imine–Enamine System: Substitution at Nitrogen *102*
5.5 Tautomer Ratio in the Imine–Enamine System: Substitution at Carbon *105*
5.6 The Resonance Contribution to Ketone and Amide Tautomerism *107*
5.7 The Field-Resonance Balance in Vinylogous Heteroaromatic Amidines *108*
5.8 Conclusions *110*
References *111*

6 Theoretical Consideration of In-Solution Tautomeric Equilibria in Relation to Drug Design *113*
Peter I. Nagy
6.1 Introduction *113*
6.2 Methodology *114*
6.2.1 General Issues *114*
6.2.2 Relative Solvation Free Energy *115*
6.2.3 Calculation of the Equilibrium Constant *117*
6.3 Equilibration Mechanism *119*

6.4 Relation to Drug Design *123*
6.4.1 Ligand Binding *123*
6.4.2 Drug Partitioning *125*
6.5 In-solution Equilibrium Calculations *127*
6.5.1 Neutral Systems *128*
6.5.1.1 Heterocyclic Tautomers *128*
6.5.1.2 Amino Acids and Aminophenols *135*
6.5.1.3 Keto–Enol Tautomerism *138*
6.5.1.4 Miscellaneous Systems *140*
6.5.2 Tautomeric Protonation *141*
6.6 Concluding Remarks *142*
References *143*

7 Direct Observation and Control of Single-Molecule Tautomerization by Low-Temperature Scanning Tunneling Microscopy *147*
Takashi Kumagai and Leonhard Grill
7.1 Brief Introduction to STM *148*
7.1.1 Operation Principle of STM *148*
7.1.2 Theoretical Model of STM *149*
7.1.3 Scanning Tunneling Spectroscopy *149*
7.1.4 Inelastic Electron Tunneling Process *151*
7.2 Direct Observation of Single-Molecule Tautomerization Using STM *152*
7.2.1 Tautomerization within Porphyrin and Phthalocyanine Derivatives *152*
7.2.2 Tautomerization within a Single Porphycene Molecule *155*
7.2.2.1 Introduction *155*
7.2.2.2 Adsorption Structure of a Porphycene Molecule on a Cu(110) Surface *156*
7.2.2.3 Thermally Induced *cis*–*cis* Tautomerization *157*
7.2.2.4 STM-Induced *cis*–*cis* Tautomerization *159*
7.2.2.5 Mechanism of STM-Induced Tautomerization *163*
7.2.2.6 Control of Tautomerization with Single Copper Atoms *166*
7.2.2.7 Tautomerization of Individual Porphycene Molecules in Molecular Assemblies *170*
7.3 Concluding Remarks *172*
Acknowledgments *172*
References *172*

8 Switching of the Nonlinear Optical Responses of Anil Derivatives: From Dilute Solutions to the Solid State *175*
Frédéric Castet and Benoît Champagne
8.1 Introduction *175*
8.2 Experimental and Theoretical Methods *178*

8.2.1 Nonlinear Optical Properties of Molecular Compounds and Solids *178*
8.2.2 Experimental Measurements of Quadratic Molecular Hyperpolarizabilities *179*
8.2.3 Calculations of Molecular Quadratic Hyperpolarizabilities *181*
8.2.4 Calculations of Second-Order Nonlinear Susceptibilities of Molecular Solids *185*
8.3 Second-Order Nonlinear Optical Responses of Anils *187*
8.3.1 NLO Responses of Anils in Solution: Structure–Property Relationships *187*
8.3.2 Solvent Effects on the NLO Switching Properties of Anils *191*
8.3.3 Switching in the Solid State: Impact of Intermolecular Interactions on the NLO Responses *193*
8.4 Conclusions *196*
Acknowledgments *197*
References *197*

9 Tautomerism in Oxoporphyrinogens and Pyrazinacenes *203*
Jonathan P. Hill, Jan Labuta, Shinsuke Ishihara, Gary J. Richards, Yongshu Xie, Francis D'Souza, and Katsuhiko Ariga
9.1 Introduction *203*
9.2 Tautomerism in Oxoporphyrinogen, OxP *205*
9.3 Multichromic Acidity Indicator Involving Tautomerism *211*
9.4 Polytautomerism in Oxocorrologen, OxC *212*
9.5 Tautomerism in Linear Reduced Fused Oligo-1,4-pyrazines (Pyrazinacenes) *219*
9.6 Conclusion *225*
References *226*

10 Enolimine–Ketoenamine Tautomerism for Chemosensing *229*
Alexander D. Dubonosov, Vladimir A. Bren, and Vladimir I. Minkin
10.1 Introduction *229*
10.2 Prototropic Enolimine–Ketoenamine Tautomerism *229*
10.3 Ionochromic Enolimine–Ketoenamine Tautomeric Systems for Ions Sensing *234*
10.4 Concluding Remarks *247*
Acknowledgments *247*
References *247*

11 Tautomerizable Azophenol Dyes: Cornerstones for Advanced Light-Responsive Materials *253*
Jaume Garcia-Amorós and Dolores Velasco
11.1 Azobenzene-Based Light-Sensitive Materials *253*
11.2 Azophenols: Tautomerizable Photochromes with Fast Switching Speeds *255*

11.2.1 Thermal Isomerization Kinetics of Azophenols in Isotropic Solvents *256*
11.2.2 Thermal Isomerization Kinetics of Azophenols in Liquid-Crystalline and Glassy Media *259*
11.3 Sub-Millisecond Thermally Isomerizing Azophenols for Optically Triggered Oscillating Materials *262*
11.4 Fast-Responding Artificial Muscles with Azophenol-Based Liquid Single Crystal Elastomers *266*
11.5 Conclusion *268*
References *269*

12 Controlled Tautomerism: Is It Possible? *273*
Daniela Nedeltcheva-Antonova and Liudmil Antonov
12.1 Introduction *273*
12.2 Manipulation of Electronic Properties of the Substituents *275*
12.3 Tautomeric Tweezers *278*
12.4 Tautomeric Cavities *279*
12.5 Proton Cranes *282*
12.6 Rotary Switches *290*
12.7 Concluding Remarks *291*
Acknowledgments *291*
References *291*

13 Supramolecular Control over Tautomerism in Organic Solids *295*
Krunoslav Užarević, Vladimir Stilinović, and Mirta Rubčić
13.1 Crystal Engineering and Tautomerism in Molecular Solids *297*
13.2 Supramolecular Synthons *298*
13.3 Solid-State Tautomerism, Proton Transfer, and Hydrogen Bonding *300*
13.4 Supramolecular Stabilization of Metastable Tautomers *304*
13.5 Identification of Tautomeric Properties and Connectivity Preferences *305*
13.6 Synthetic Methods *306*
13.7 Supramolecular Interactions in Other Tautomeric Solids *310*
References *324*

14 Proton Tautomerism in Systems of Increasing Complexity: Examples from Organic Molecules to Enzymes *329*
Hans-Heinrich Limbach, Gleb S. Denisov, Ilya G. Shenderovich, and Peter M. Tolstoy
14.1 Introduction *329*
14.2 Hydrogen Bond Geometries and Proton Transfer *330*
14.3 Tautomerizations without Requiring Reorganization of the Environment *333*

14.3.1 Examples of Intramolecular Tautomerizations without Requiring Reorganization of the Environment *334*
14.3.2 Examples of Intermolecular Tautomerizations in the Absence of Pre-Equilibria without Requiring Major Reorganization of the Environment *338*
14.3.3 Examples of Intermolecular Tautomerizations in the Presence of Pre-Equilibria without Requiring Major Reorganization of the Environment *340*
14.3.4 Mechanisms of Tautomerizations without Requiring Reorganization of the Environment *342*
14.3.5 An Application to the Function of the Imidazole Ring of Histidine 64 in Human Carbonic Anhydrase II *344*
14.4 Tautomerizations Requiring Reorganization of the Environment *346*
14.4.1 Tautomerization of Charged Molecules and Hydrogen Bonded Clusters *347*
14.4.1.1 Proton Sponges *347*
14.4.1.2 Phenol–Carboxylate versus Carboxylic Acid–Phenolate Complexes *351*
14.4.1.3 Homoconjugated Carboxylic Acid Carboxylates *354*
14.4.2 Tautomerization of Neutral Heterocyclic Acid–Base Complexes *356*
14.4.2.1 Model Complexes of the Acid–Pyridine Type *356*
14.4.2.2 Mannich Bases *358*
14.4.2.3 Model Schiff Bases *359*
14.4.2.4 The Cofactor Pyridoxal 5′-phosphate: from Organic Models to Alanine Racemase and Aspartate Aminotransferase *360*
14.5 Conclusions *364*
Acknowledgments *365*
References *365*

Index *373*

List of Contributors

Liudmil Antonov
Institute of Organic Chemistry
Bulgarian Academy of Sciences
Acad. G. Bonchev street, bl. 9
Sofia 1113
Bulgaria

Katsuhiko Ariga
Supermolecules Group
WPI Center for Materials
Nanoarchitectonics
National Institute for Materials
Science
Namiki 1-1, Tsukuba
Tsukuba
Ibaraki 305-0044
Japan

Thomas Bally
University of Fribourg
Department of Chemistry
Chemin du Musée 9
1700 Fribourg
Switzerland

Vladimir A. Bren
Southern Federal University
Institute of Physical and Organic
Chemistry
194/2 Stachka Av.
344090 Rostov on Don
Russian Federation

Frédéric Castet
Université de Bordeaux
Institut des Sciences
Moléculaires (ISM, UMR 5255
CNRS)
351 Cours de la Libération
33405 Talence Cedex
France

Benoît Champagne
Université de Namur (UNamur)
Laboratoire de Chimie Théorique
UCPTS, Département de Chimie
Rue de Bruxelles 61
5000 Namur
Belgium

Francis D'Souza
Univeristy of North Texas
Department of Chemistry
1155 Union Circle
305070 Denton
Texas 76203
USA

Gleb S. Denisov
St. Petersburg State University
Institute of Physics
198504 St. Petersburg
Russian Federation

Alexander D. Dubonosov
Southern Scientific Center of
Russian Academy of Sciences
Department of Physical and
Organic Chemistry
41 Chekhov St.
344006 Rostov on Don
Russian Federation

José Elguero
Instituto de Química Médica
Juan de la Cierva, 3
28006 Madrid
Spain

Jaume Garcia-Amorós
Universitat de Barcelona
Institut de Nanociència i
Nanotecnologia (IN^{2}UB)
Grup de Materials Orgànics
Departament de Química
Orgànica
Martí i Franqués 1
08028 Barcelona
Spain

Leonhard Grill
University of Graz
Department of Physical
Chemistry
Heinrichstrasse 28
8010 Graz
Austria

Poul Erik Hansen
Roskilde University
Department of Science
and Environment
Building 28
Universitetsvej 1
DK-4000 Roskilde
Denmark

Jonathan P. Hill
Supermolecules Group
WPI Center for Materials
Nanoarchitectonics
National Institute for Materials
Science
Namiki 1-1, Tsukuba
Ibaraki 305-0044
Japan

Shinsuke Ishihara
Supermolecules Group
WPI Center for Materials
Nanoarchitectonics
National Institute for Materials
Science
Namiki 1-1, Tsukuba
Ibaraki 305-0044
Japan

Takashi Kumagai
Fritz-Haber Institute of the
Max-Planck Society
Department of Physical
Chemistry
Faradayweg 4-6
14195 Berlin
Germany

Jan Labuta
International Center for Young
Scientists
National Institute for Materials
Science
Sengen 1-2-1, Tsukuba
Ibaraki 305-0047
Japan

Hans-Heinrich Limbach
Institut für Chemie und
Biochemie der Freien Universität
Berlin
Takustrasse 3
14195 Berlin
Germany

Vladimir I. Minkin
Southern Federal University
Institute of Physical and Organic
Chemistry
194/2 Stachka Av.
344090 Rostov on Don
Russian Federation

Peter I. Nagy
The University of Toledo
College of Pharmacy and
Pharmaceutical Sciences
Center for Drug Design and
Development
2801 West Bancroft Street
Toledo, OH 43606-3390
USA

Daniela Nedeltcheva-Antonova
Institute of Organic Chemistry
Bulgarian Academy of Sciences
Acad. G. Bonchev street, bl. 9
Sofia 1113
Bulgaria

Gary J. Richards
Ochanomizu University
Department of Chemistry
Faculty of Science
2-1-1 Otsuka
Bunkyo-ku
Tokyo 112-8610
Japan

Mirta Rubčić
University of Zagreb
Department of Chemistry
Faculty of Science
Horvatovac 102a
10000 Zagreb
Croatia

Ilya G. Shenderovich
University of Regensburg
Universitätsstr. 31
93040 Regensburg
Germany

Vladimir Stilinović
University of Zagreb
Department of Chemistry
Faculty of Science
Horvatovac 102a
10000 Zagreb
Croatia

Peter J. Taylor
AstraZeneca
Alderley Park, Macclesfield
Cheshire
UK

Peter M. Tolstoy
St.Petersburg State University
Center for Magnetic Resonance
Universitetsky pr. 26
198504 St. Petersburg
Russian Federation

Krunoslav Užarević
Ruđer Bošković Institute
Division of Physical Chemistry
Bijenička Cesta 54
10000 Zagreb
Croatia

and

McGill University
Department of Chemistry
801 Sherbrooke Street West
QC H3A 0B8
Canada

Dolores Velasco
Universitat de Barcelona
Institut de Nanociència i Nanotecnologia (IN^2UB)
Grup de Materials Orgànics
Departament de Química Orgànica
Martí i Franqués 1
08028 Barcelona
Spain

Yongshu Xie
East University for Science and Technology (ECUST)
Key Laboratory for Advanced Materials and Institute of Fine Chemicals
130 Meilong Road
Shanghai 200237
P.R. China

Preface

According to the UIPAC definition [1], tautomerism is "Isomerism of the general form:

$$\text{G-X-Y} = \text{Z} \rightleftarrows \text{X} = \text{Y-Z-G}$$

where the isomers (called *tautomers*) are readily interconvertible; the atoms connecting the groups X, Y, and Z are typically any of C, N, O, or S, and G is a group that becomes an electrofuge or nucleofuge during isomerization. The commonest case, when the electrofuge is H^+, is also known as *prototropy*." And while "tautomerism" usually means existing equilibrium, with the term *proton transfer* the dynamics of the prototropic tautomerism is usually marked.

Under these arid definitions an interesting tautomeric world is covered. Tautomers are the chameleons of chemistry [2, 3], capable of changing by a simple change of phase from an apparently established structure to another (not perhaps until then suspected), and then back again when the original conditions are restored, and of doing this in an instant: intriguing, disconcerting, and perhaps at times exasperating. And a change in structure means changes in properties as well.

The last sentence expresses the idea of the current book. It differs from "Tautomerism: Methods and Theories" [3], where the theoretical and methodological base of tautomerism has been systematically described. This book deals with ***applications.*** Most of them are potential, but they give ideas and show how these ideas have been developed. Actually, these potential applications are promises that the tautomeric field of research gives for future technologies. The latest achievements, presented here, include: applicability of tautomeric compounds as sensors (Chapters 9 and 10) and switches (Chapter 8); manipulation of tautomeric properties in solution (Chapter 12) and solid state (Chapter 13); and observing individual tautomers by scanning tunneling microscopy (Chapter 7), using tautomerism in the drug design (Chapter 6) and optical information processing (Chapter 11).

Returning back to the past, my generation has had a chance either to work together or to learn from a generation of great scientists, by whom tautomerism has been developed as a well-established research field, as a system of scientific ***concepts.*** The main feature of these "tautomeric" pioneers is that they have always been experimentalists and theoreticians simultaneously, which brought a balanced view and in-depth interpretation of each tautomeric case they

investigated. There is a special spirit that can be felt from reading their papers, a unique knowledge and experience that we, the younger generations, are obligated to keep. This is one more reason for the current book, concepts are presented in Chapters 1-5 and 14.

Many names can be listed here and some of them can be easily recognized from among the contributors. Two of them, Jose Elguero and Hans-Heinrich Limbach, have written the first and the last chapter of this book. Peter J. Taylor, who passed away in 2012, was the catalyst for the book "Tautomerism: Methods and Theories", and until his last days was discussing with me the content and the scope of this second book. His sketches and ideas are now Chapters 2 and 5 and in the process of adapting them I have discovered that it is not true that there is no experimental information concerning tautomeric systems, as often theoreticians complain. There is a lot of information that waits to be rediscovered and explained theoretically. There are many intriguing tautomeric cases waiting for new experiments. There are many promising applications. There are a lot of opportunities.

Tokyo-Sofia, 2015

References

1. Muller, P. (1994) *Pure Appl. Chem.*, **66**, 1077–1184.
2. Martin, Y.C. (2009) *J. Comput. Aided Mol. Des.*, **23**, 693–704.
3. Antonov, L. (ed.) (2014) *Tautomerism: Methods and Theories*, Wiley-VCH Verlag GmbH.

14
Proton Tautomerism in Systems of Increasing Complexity: Examples from Organic Molecules to Enzymes

Hans-Heinrich Limbach, Gleb S. Denisov, Ilya G. Shenderovich, and Peter M. Tolstoy

14.1
Introduction

The term *tautomerism* has been defined by IUPAC as [1] isomerism of the general form

$$G - X - Y = Z \rightleftarrows X = Y - Z - G \tag{14.1}$$

where the isomers (called *tautomers*) are readily interconvertible; the atoms connecting the groups X, Y, Z are typically any of C, H, O or S, and G is a group that becomes an electrofuge or nucleofuge during isomerization. The commonest case, when the electrofuge is H+, is also known as *prototropy*. The definition of "electrofuge" is: "a leaving group that does not carry away the bonding electron pair." Moreover, "The grouping Y may itself be a three-atom (or five-atom) chain extending the conjugation. The double bond between Y and Z may be replaced by a ring, when the phenomenon is called *ring-chain tautomerism*."

In contrast to this definition we will consider in this review also other molecular systems or complexes containing hydrogen species H, which can move between different locations. Thus, we include systems exhibiting an aliphatic chain as link between the two atoms, that is,

$$H - X - Y - Z \rightleftarrows X - Y - Z - H \tag{14.2}$$

or acid–base complexes that are stable within the time scale of the spectroscopic method used and in which a hydrogen transfer takes place:

$$A - H \cdots B \rightleftarrows A \cdots H - B. \tag{14.3}$$

When H carries a positive charge, Eq. (14.3) will correspond to a proton transfer, typically from an acid to a base.

As in Eq. (14.1), the question of charge transfer accompanying the H transfer is left open. Therefore, H in Eqs. (14.2) and (14.3) may represent either a proton, a hydrogen atom, or a hydride species.

Tautomerism: Concepts and Applications in Science and Technology, First Edition.
Edited by Liudmil Antonov.

But generally, tautomerizations will either constitute or be part of very complex processes, requiring hydrogen bond switching, counterion motions, solvent reorganization, or possibly a catalyst.

In this contribution, we will successively discuss examples of proton tautomerism with an increasing degree of reaction complexity, starting from intramolecular hydrogen transfers and ending with complex proton transfers in enzymes. All examples have been studied experimentally using various methods of dynamic NMR spectroscopy [2].

14.2
Hydrogen Bond Geometries and Proton Transfer

In this section, we will shortly describe some important geometrical features of hydrogen bonding and proton transfer, which have been reviewed recently [3, 4]. One can associate to any hydrogen-bonded system A–H···B two distances $r_1 = r_{AH}$ and $r_2 = r_{HB}$ as illustrated in Figure 14.1. It is convenient to define additionally the natural hydrogen bond coordinates q_1 and q_2.

$$q_1 = {}^1\!/_2(r_1 - r_2), \quad q_2 = r_1 + r_2. \tag{14.4}$$

In the case of a linear hydrogen bond, q_1 corresponds to the distance of the proton with respect to the hydrogen bond center and q_2 to the heavy atom A···B distance.

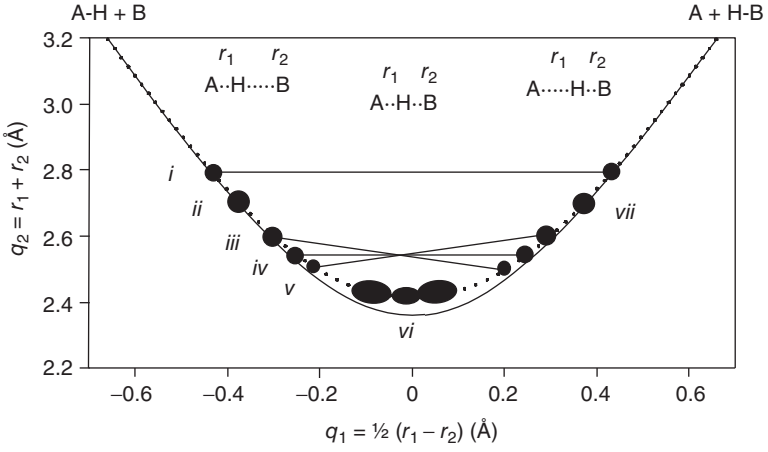

Figure 14.1 Correlation of the hydrogen bond length $q_2 = r_1 + r_2$ with the proton transfer coordinate $q_1 = 1/2(r_1 - r_2)$ according to [5]. Solid line: correlation for equilibrium distances of the OHO hydrogen bonds of water clusters. Dotted line: empirical correction for zero-point vibrations. (*i*) Degenerate tautomerism in a weak hydrogen bond exhibiting an equilibrium constant of $K = 1$. (*ii*) and (*vii*) System without tautomerism. (*iii*) to (*v*) Nondegenerate tautomerizations exhibiting equilibrium constants of $K < 1$ to $K > 1$. (*vi*) Geometries of low- or no-barrier asymmetric hydrogen bonds.

According to the valence bond order concept of Pauling [6] one can associate to both hydrogen bond distances valence bond orders given by

$$p_1 = \exp\{-(r_1 - r_1^\circ)/b_1\} \text{ and } p_2 = \exp\{-(r_2 - r_2^\circ)/b_2\} \tag{14.5}$$

where r_1° and r_2° represent the equilibrium distances in the fictive free diatomic units AH and HB, and b_1 and b_2 describe bond order decays with increasing bond distances.

As the total valency of hydrogen is unity, it follows that

$$p_1 + p_2 = \exp\{-(r_1 - r_1^\circ)/b_1\} + \exp\{-(r_2 - r_2^\circ)/b_2\} = 1. \tag{14.6}$$

Thus, both distances r_1 and r_2 depend on each other, that is, q_1 depends on q_2 and vice versa. The resulting "equilibrium" correlation for OHO hydrogen bonds is depicted in Figure 14.1 as a solid line. The necessary parameters were adapted to water cluster structures calculated using DFT methods [5]. The curve indicates that the shift of H toward the hydrogen bond center is accompanied by a hydrogen bond compression, which is maximum when H is located in the center. Following this the H-bond widens again. In other words, hydrogen bond formation and proton transfer can be described simultaneously by a single coordinate. The correlation curve has been supported for OHO, OHN, NHN hydrogen bonds by DFT calculations and is valid not only for neutral but also for charged systems. However, the neglect of the kinetic energy of nuclei in *ab initio* calculations implies that a nucleus can be represented by a single set of coordinates in space. In reality, zero-point motions imply in particular for hydrogen isotopes a minimum volume or "shape."

This leads to deviations of observed hydrogen bond correlations as compared to equilibrium correlations as illustrated in Figure 14.1 by the dotted line which was adapted to experimental OHO-hydrogen bond geometries determined from neutron diffraction data [7] and dipolar solid state NMR [8, 9] of systems for which no tautomerism could be detected. In particular, it was observed that in the case of very strong hydrogen bonds around $q_1 = 0$ the shortest heavy atom distance $q_{2_{\min}}$ was not reached [5, 10, 11]. The deviations depend on the type of molecular systems. As the zero-point vibrations depend on the hydrogen isotope they result in geometric H/D isotope effects [3].

We note that very often "short" hydrogen bonds exhibiting values of q_2 near the minimum value are considered as "strong" and "long" hydrogen bonds as weak. We will use this wording during this review.

In Figure 14.1 some typical situations of tautomeric system are schematically depicted. A tautomer is characterized not only by a mole fraction as illustrated by the size of the filled circles but also by an average hydrogen bond geometry representing a point in the correlation diagram. Situation *i* refers to a degenerate tautomerism in a weak hydrogen bond exhibiting an equilibrium constant of tautomerism, $K = 1$. The two tautomers exhibit the same value of the heavy atom coordinate q_2. In the case of nonsymmetric hydrogen bonds of medium strength the equilibrium constants will be generally different from 1. Thus, *ii* and *vii* correspond to situations where only one tautomer is formed in each case. *iii* to *v*

correspond to situations of an asymmetric system with $K < 1$, $K = 1$, and $K > 1$. We note that two interconverting tautomers may exhibit different values of q_2. It will be shown later that the nondominant tautomer generally exhibits a shorter hydrogen bond as expressed by a smaller value of q_2 as compared to the dominant one. Finally, *vi* reflects the situation of a very strong asymmetric low- or no-barrier hydrogen bond.

In order to obtain hydrogen bond geometries in liquid or soft matter environments efforts have been made to set up correlations between these geometries and NMR parameters of the nuclei of the hydrogen bridges or of nearby nuclei. The most important ones are the ^{1}H chemical shifts of the hydrogen-bonded proton, the chemical shifts of the bridge or nearby nuclei, and the scalar coupling constants between the bridge nuclei across the hydrogen bonds [3, 5, 12, 13]. In addition, intrinsic isotope effects on the corresponding NMR chemical shifts have been described to arise from geometric H/D isotope effects. Generally, correlations of NMR parameters with hydrogen bond geometries work well for strong hydrogen bonds whereas the influence of the chemical structure needs to be considered when hydrogen bonds of medium strength or weak hydrogen bonds are discussed. As this problem of hydrogen bond geometries and NMR parameters is beyond the scope of this review we refer the reader to the original literature whenever examples are discussed in this chapter.

In most cases of weak or moderately strong hydrogen bonds the proton will not transfer along the dashed lines in Figure 14.1, but firstly a hydrogen bond compression will occur, which then strongly reduces the barrier of proton transfer. This will require a compression energy. Proton transfer will occur then at a given heavy atom distance where the total barrier is minimized. Thus, before the proton transfer, heavy atom reorganization takes place, which strengthens the hydrogen bond. The transfer itself may occur via incoherent tunneling through the barrier or hopping over the barrier. In the case of proton tunneling, some heavy atom motions will also occur. For example, in the case of Eq. (14.1) the X–Y bond will be shortened and the Y–Z bond lengthened [14].

In the region of strong hydrogen bonds where the solid and dotted correlation curves as depicted in Figure 14.1 are different, intrinsic H/D isotope effects result, better dubbed as geometric H/D isotope effects as illustrated schematically in Figure 14.2. Generally, exchange of H for D results in a shortening of the covalent and a lengthening of the hydrogen bond [15]. The one-dimensional potential energy curves indicate that the different anharmonic vibrational wave functions (squares) are at the origin of this effect. In the case of the strongest hydrogen bond a difference occurs depending on the height of the potential barrier separating the two wells. If the barrier is larger than the zero-point energy, generally H is more confined in the hydrogen bond center as compared to D, resulting in a shorter A … B distance (Figure 14.2a). By contrast, when the barrier is very small the A· · ·B distance is smaller in the deuterated hydrogen bond because the volume of D is smaller than of H, and hence D is located closer in the hydrogen bond center (Figure 14.2b). As illustrated in Figure 14.2c, a third possibility is a fast degenerate interconversion of slightly asymmetric single well configurations

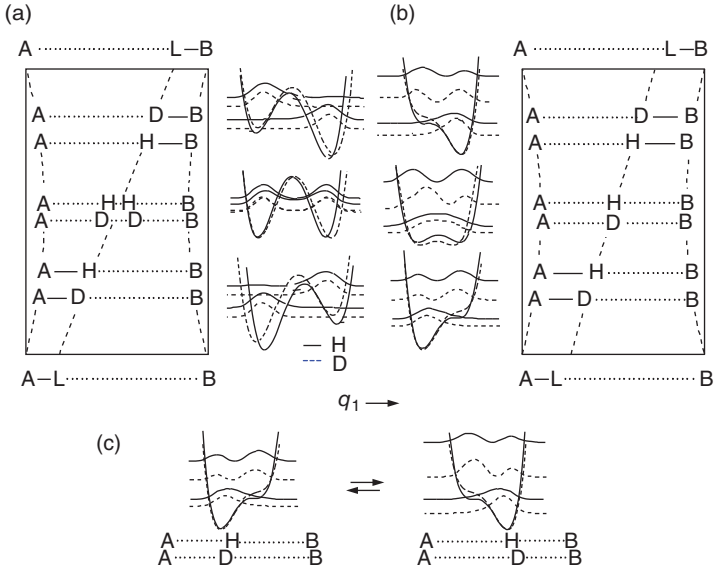

Figure 14.2 One-dimensional hydron potentials and geometric changes during the transfer of a hydron L = H or D from A to B (schematically). The squares of the wave functions of some vibrational states for H and D, that is, the proton and deuteron distribution functions are included. (a) A small barrier at the quasisymmetric midpoint leads to a small normal H/D isotope effect on the hydrogen bond geometry. An inverse effect appears in case (b) exhibiting a very low barrier. (c) The quasi-symmetric situation in (a) can also be realized by a fast equilibrium between asymmetric configurations exhibiting a different solvent shell.

arising from a distribution of different solvent shells [16] which have also been called *solvatomers* [17]. How proton transfer and hence tautomerizations are influenced by the environment is a major question whose answers depend on the molecular system studied as shown in the next sections.

14.3
Tautomerizations without Requiring Reorganization of the Environment

Tautomerizations that are not accompanied by large electrostatic changes between the initial and final states do not require major reorientations of neighboring molecules. In these cases, hydrogen nuclei are transferred from one heavy atom to another as supposed in Eq. (14.1). Major electrostatic changes are avoided because the heavy atoms are linked via a number of conjugated double bonds. This implies the possibility of electronic reorganization during a tautomerization. Thus the initial and final states are generally neutral although minor dipole moment changes can occur. In other words, not only protons but also electrons are moved, and these reactions have, therefore, been dubbed as "hydrogen transfers" and not as "proton transfers."

A consequence is that such tautomerizations can not only take place in the liquids but often also in the solid state. The reaction barriers depend strongly on the heavy atom distances q_2 and the energy needed for their compression. The occurrence of major electrostatic changes in the transition or intermediate states will only lead to a barrier increase which might, however, be substantial. In the following examples, different reaction types are discussed, which have been studied using dynamic liquid and solid state NMR.

14.3.1
Examples of Intramolecular Tautomerizations without Requiring Reorganization of the Environment

In this section we will discuss some typical examples exhibiting intramolecular tautomerizations whose kinetics have been studied by dynamic NMR in various environments. Often, the gas phase and liquid state degeneracies were found to be slightly disturbed in the solid state. In most cases, nonlinear Arrhenius curves were observed, which indicated the role of vibrationally assisted tunneling, supported in almost all cases by the observation of nonclassical kinetic isotope effects.

N,*N*′-Diphenyl-6-aminofulvene-1-aldimine **1** (Figure 14.3) exhibits an intramolecular NHN hydrogen bond of medium strength and a very fast solid

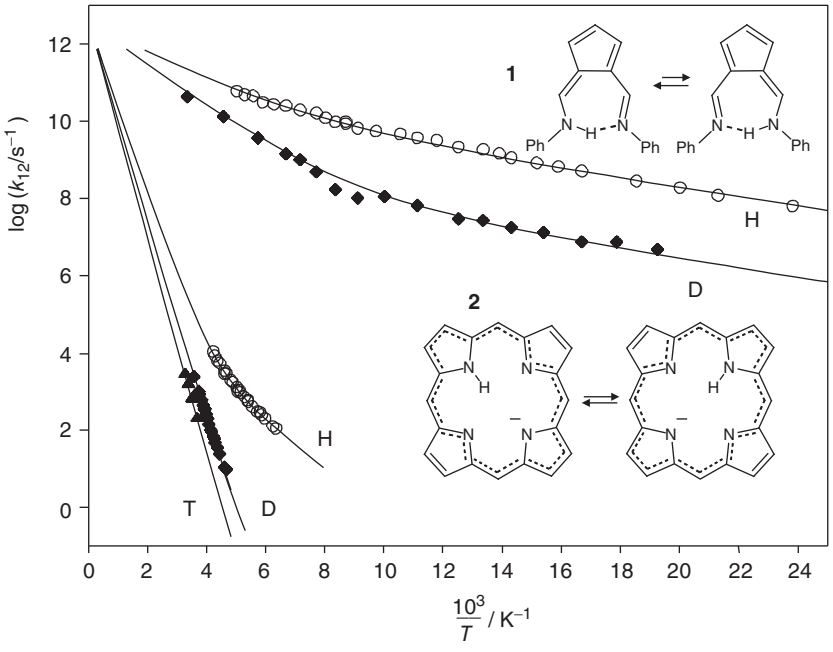

Figure 14.3 Top: Arrhenius diagram of the H- and D-tautomerization of *N*,*N*′-diphenyl-6-aminofulvene-1-aldimine **1** in the solid amorphous state. (Adapted from [18].) Bottom: Arrhenius diagram of the H-, D-, T-tautomerization of the porphyrin anion **2**. (Reproduced from Braun *et al.* [19]. Copyright (1994), with permission of Wiley.)

state tautomerism in the nanosecond timescale which has been observed by NMR spectroscopy and relaxometry [18]. The equilibrium constants were close to but not unity arising from solid state effects. The rate constants and kinetic H/D isotope effects were found to be different for the polycrystalline and an amorphous state. The Arrhenius diagram for the amorphous solid is depicted in Figure 14.3; the Arrhenius curves exhibit concave curvature and at low temperatures temperature-independent isotope effects. By contrast, the reaction rates were much slower in the case of the aromatic porphyrin anion **2** for which temperature-dependent kinetic H/D/T isotope effects were reported [19, 20]. The Arrhenius diagram of **2** is also included in Figure 14.3. No liquid–solid state effects were observed and the gas phase degeneracy was maintained in solution and the solid state. This means that inspite of the negative charge and potential cation–anion interactions electrostatics is not a major issue in the tautomerization of the anion.

In a similar way, as the hydrogen transfer sites of porphyrin **3** (Figure 14.4) and its derivatives are well embedded inside the molecules also, none or only small liquid–solid state effects were observed [21, 22] as long as the equilibrium constants remained unity. The hydrogen bonds are very weak or even nonexistent and the hydrogen transfer is of the order of milliseconds. The full kinetic hydrogen/deuterium/tritium isotope effects indicated a stepwise tautomerization via a *cis*-intermediate of high energy. For that reason, the tautomerization of porphyrin is slower than that of its anion.

As illustrated by the dashed lines, porphyrin **3** constitutes an 18 π-electron system with two peripheral double bonds that move during the tautomerization. This feature results from finding the inner protons of **3** at high field around −3.5 ppm [21], typical for protons located inside an aromatic ring. When one or both peripheral double bonds on opposite pyrrole rings are hydrogenated leading to the hydroporphyrins chlorin **4** and bacteriochlorin **5** (Figure 14.4), no essential low-field shift of the inner protons occurs supporting the aromatic pathways of **3**. However, a substantial low-field shift is observed when two outer double bonds in adjacent pyrrole rings are hydrogenated leading to iso-bacteriochlorin **6** [23], which indicates that it has lost its aromatic character. The hydrogenation of the peripheral double bonds strongly influences the tautomerism. The rates of the intramolecular proton exchange of **4** are smaller than of **3** because only the first *trans*-tautomer is aromatic, whereas the second *trans*-tautomer has lost its aromaticity and exhibits a higher energy. It is only observable as an intermediate of the exchange of the two inner protons [24]. By contrast, **5** does not exhibit an observable inner proton exchange because the second *trans*-tautomer is expected to be zwitterionic as illustrated in Figure 14.4.

For **6,** two different tautomerizations were observed – a fast "vertical" one and a slow "horizontal" one [23] (Figure 14.4). In the latter, the molecule remained nonaromatic during the reaction whereas the fast vertical process could be explained in terms of an aromatic intermediate as illustrated in Figure 14.4. This lowers the energy of the intermediate and hence of the corresponding

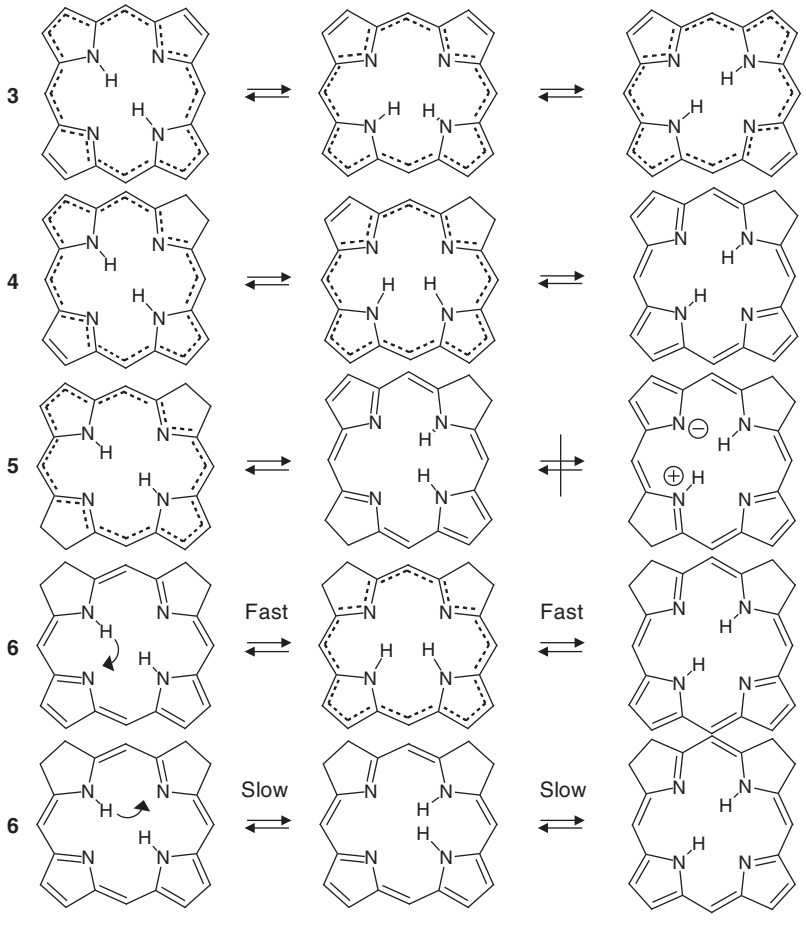

Figure 14.4 Tautomerization of porphyrin **3** [21, 22] and the hydroporphyrins chlorine **4**, bacteriochlorin **5,** and iso-bacteriochlorin **6** [23] in the liquid state.

transition states and demonstrates the influence of the molecular structure on the tautomerization barriers.

The tautomerization of solid phthalocyanine **7** (Figure 14.5) is somewhat faster than that of **3**, a finding which has been attributed to the formation of weak intramolecular hydrogen bonds as the molecular skeleton can be deformed easily as compared to porphyrins [25]. Stronger hydrogen bonds are observed in substituted tetraaza[14]annulenes **8** [26, 27] and the tautomerizations are faster. This trend is enhanced in the case of porphycene **9** and its derivatives [28–31]. In contrast to **6**, only the "vertical" tautomerization is observed but not the "horizontal" one as only the first process is assisted by hydrogen bond formation. Note that the tautomerizations of porphycene and its substituted analogs have not only been studied by NMR but also by using optical methods [32].

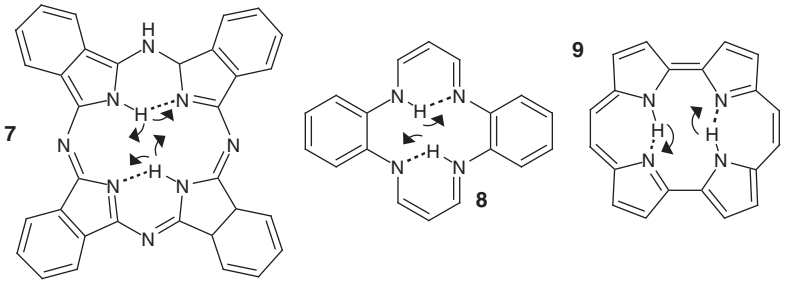

Figure 14.5 Tautomerization of solid phthalocyanine **7** [25], tetraaza[14]annulene **8** [26, 27], and porphycene **9** [28, 29]. The arrows indicate hydrogen transfers.

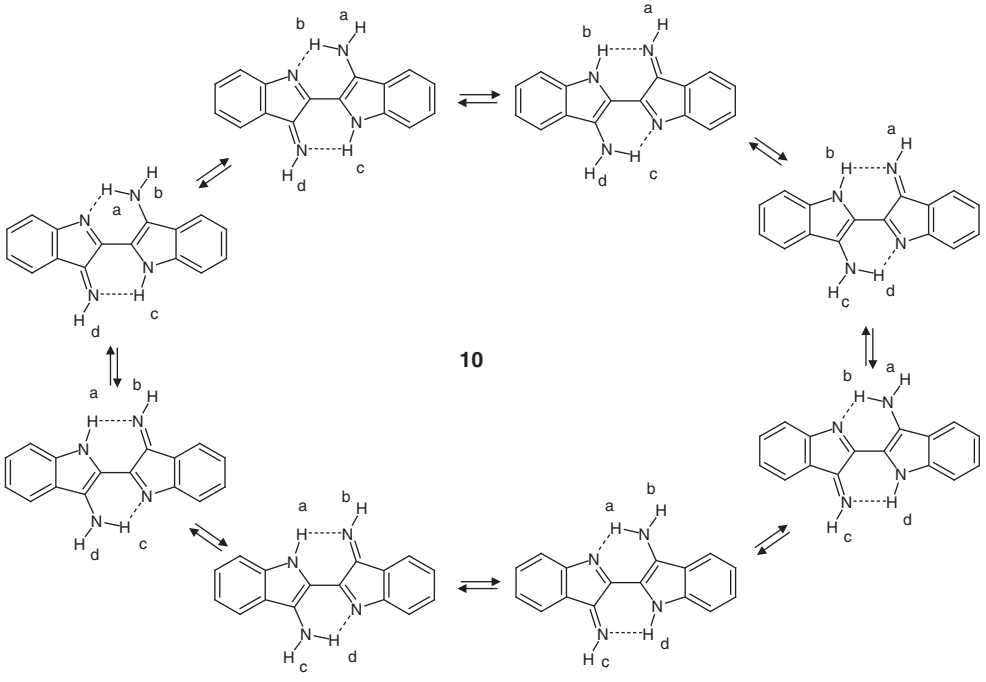

Figure 14.6 Coupled degenerate double proton transfer and NH_2 rotation in indigodiimine **10** [33].

Tautomeric processes can be part of a more complex reaction network as is demonstrated in the case of indigodiimine **10,** which exhibits an intramolecular double proton transfer [33] illustrated in Figure 14.6. This process renders the two halves of the molecule equivalent. An even faster NH_2 rotation renders all NH protons equivalent.

The tautomerism of azophenine **11** [34, 35], of tetraphenyloxalamidine **12** [36] and of the bicyclic oxalamidines **13** and **14** [37–39] is depicted in Figure 14.7. The determination of the full kinetic HH/HD/DD isotope effects indicated stepwise

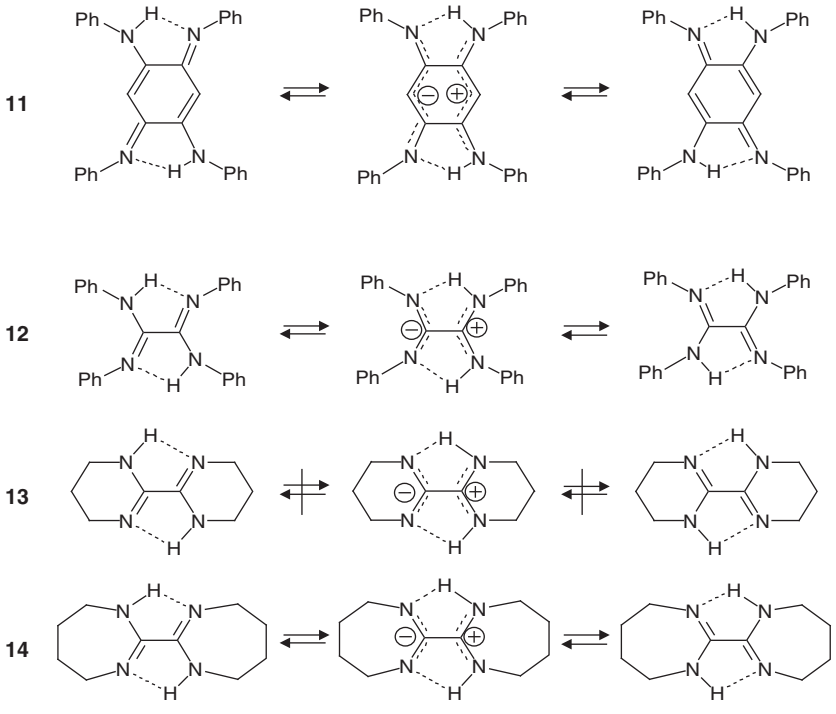

Figure 14.7 Tautomerizations of azophenine **11** [34, 35] and tetraphenyloxalamidine **12** [36]. No tautomerization is observed for the bicyclic oxalamidine **13**, but a fast tautomerization for **14** [37–39].

double proton transfers proceeding via intermediates and exhibiting large dipole moments, which correspond formally to zwitterions. Interestingly, the rate constants of **11** and **12** are almost the same but larger than those of **14**. By contrast, no tautomerization could be observed for **13**. Calculations illustrate the necessity of hydrogen bond compression to reach the zwitterionic intermediate, which requires motions of the substituents, easy for **11** and **12** but very difficult for **14**.

14.3.2 Examples of Intermolecular Tautomerizations in the Absence of Pre-Equilibria without Requiring Major Reorganization of the Environment

Molecular tautomerizations proceeding via intermolecular pathways without being assisted by catalysts can take place only in cyclic hydrogen-bonded complexes. The latter can exist as dominant species only in solids or in organic solvents, which are not hydrogen bond donors or acceptors. The latter would destroy the cyclic hydrogen-bonded complexes. Moreover, more than one proton have to be transferred to avoid charge separation that would lead to a strong coupling to the environment.

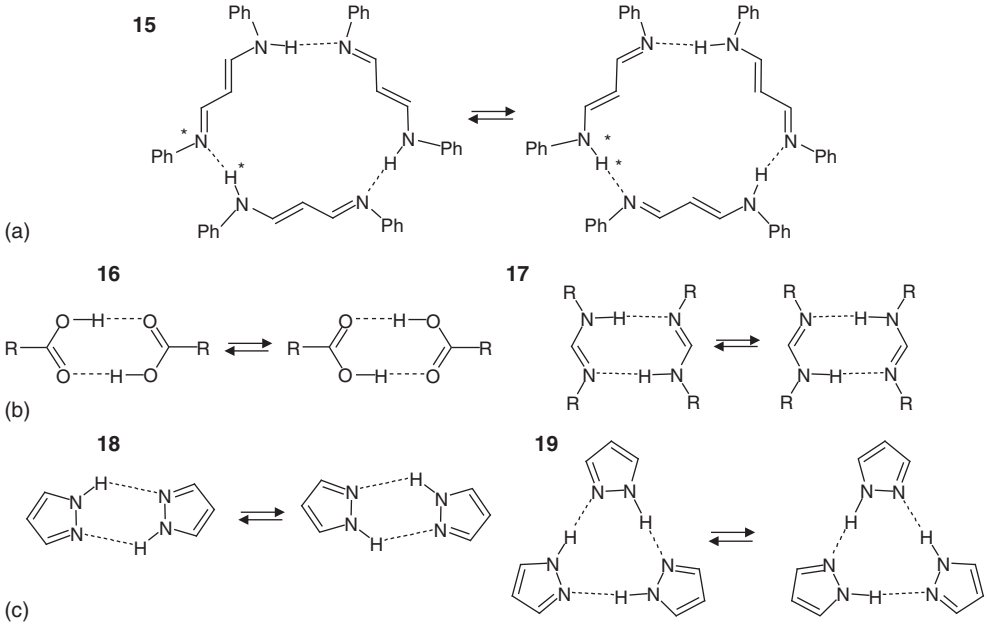

Figure 14.8 (a) Tautomerizations of the *N*,*N*-bis(pentadeuterophenyl)-1-amino-3-iminopropene trimer **15** in carbon disulfide [40, 41]. (b,c) Multiple solid state proton transfers in cyclic carboxylic acid dimers **16** [42], bis-arylformamidine dimers **17** [43], substituted pyrazole dimers **18** and trimers **19** [44].

An early example is the cyclic trimer of *N*,*N*-bis(pentadeuterophenyl)-1-amino-3-iminopropene **15**, the dianil of malonaldehyde (Figure 14.8) dissolved in CS_2. This trimer dominates at low temperature whereas at room temperature a monomer is observed [40, 41]. In the trimer a triple proton transfer is observed. With respect to a single molecule, the two other molecules constitute catalysts that accept a proton at one nitrogen site and transfer another proton to the other nitrogen site. Thus, the tautomerism is linked to an intermolecular proton transfer. The double proton transfers in solid cyclic carboxylic acids dimers **16** [42], bis-arylformamidine dimers **17** [43], substituted pyrazole dimers **18** [44], and the triple proton transfer in cyclic substituted solid pyrazole trimers **19** [44] constitute similar processes.

As discussed below, studies of the multiple kinetic hydrogen/deuterium isotope effects show that the reactions of **16**–**19** exhibit only a single barrier, involving a concerted hydrogen bond compression followed by a concerted multiple proton transfer. The different behavior of these complexes as compared to the stepwise intramolecular multiple proton transfers will be discussed later.

By contrast, the tautomerization of solid pyrazole tetramers **20** (Figure 14.9) proceeds via two consecutive concerted double proton transfers via a zwitterionic intermediate [44]. This was to be expected as a concerted hydrogen bond compression of a large number of hydrogen bonds is not feasible. On the other

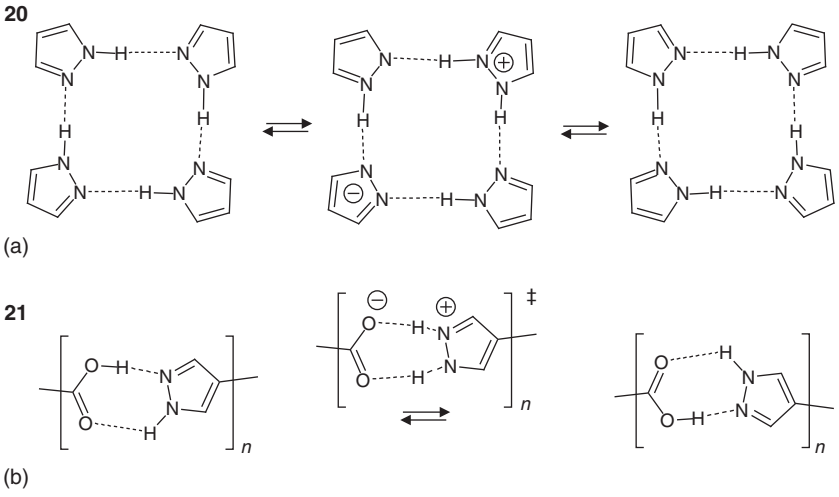

Figure 14.9 Solid state tautomerization of a substituted pyrazole tetramer **20** [44] (a) and of pyrazole-4-carboxylic acid **21** (b) [45, 46].

hand, it could not be determined whether the reaction is concerted or stepwise for linear hydrogen-bonded chains in solid pyrazole-4-carboxylic acid **21** [45, 46] but at least a zwitterionic transition state or intermediate was expected.

Finally, we note that in all cases besides the heavy atom motions leading to hydrogen bond compression as well as the minor heavy atom motions during proton tunneling no major reorganization of the environment takes place.

14.3.3
Examples of Intermolecular Tautomerizations in the Presence of Pre-Equilibria without Requiring Major Reorganization of the Environment

Some examples of intermolecular tautomerizations whose multiple kinetic isotope effects have been studied by NMR are depicted in Figure 14.10. When proton donors such as acetic acid **22** and methanol **23** are dissolved in a solvent S such as the proton acceptor tetrahydrofuran they form a hydrogen bond with the latter. The two hydrogen bonds must be broken before a cyclic hydrogen-bonded intermediate **24** can be formed in which the proton exchange takes place [47, 48]. The asterisks indicate different spin states that allow one to characterize the nuclei taking part in the exchange processes. As the hydrogen bonds in the cyclic complex are less linear and hence weaker than those to the solvent, and as the solvent concentration is large, the equilibrium constant K of the cyclic complex formation is small and hence also the proton exchange rate. The latter is first order with respect to the concentration of both proton donors, where the observed second-order rate constant $k_{obs} = Kk$. Here, k is the intrinsic rate constant in the complex.

By contrast, in the case of bis-arylformamidines **25** dissolved in tetrahydrofuran the dimerization constants K are much larger, and at high concentrations only the

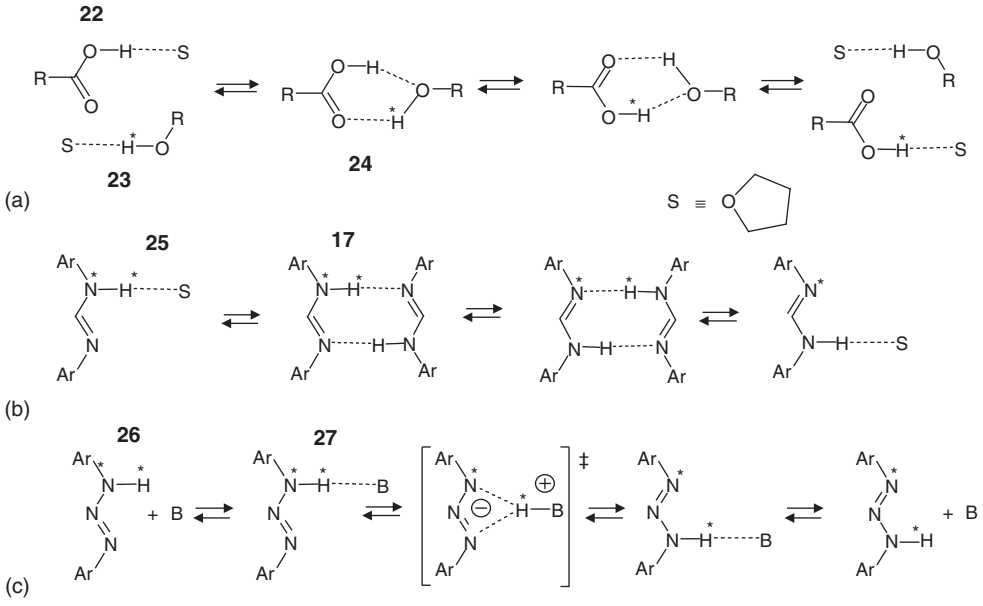

Figure 14.10 Liquid state tautomerizations requiring a pre-equilibrium. (a) Proton exchange between acetic acid **22** and methanol **23** in tetrahydrofuran. The exchange takes place in the cyclic complex **24**. The kinetic HH/HD/DD isotope effects measured by NMR indicate tunneling [47, 48]. (b) Related liquid state proton exchange of bis-arylformamidines **25** [49, 50]. The exchange takes place in the dimers of type **17** (Figure 14.8). (c) The tautomerism of bis-aryltriazene **26** [50, 51] is quenched in the liquid state without catalyst as they are not able to form cyclic dimers. A base B catalyzed intramolecular tautomerization which occurs with bases such as trimethylamine. The proton is transferred in the complex **27** temporarily to the base and then back to the original nitrogen or to the adjacent nitrogen without intermolecular proton exchange [51].

dimers **17** are present leading to a switch of the rate law from the second-order to the first order type [49, 52]. The rate constants in the complex were very similar to those found in the crystalline state [43].

An especially interesting case is bis-aryltriazene **26** [50, 51] which is not able to form cyclic dimers, in contrast to bis-arylamidines **17** [49, 52]. The crystal structures indicate a steric hindrance between the formyl CH and the aryl *o*-CH in **17**, leading to a substantial angle between the aryl groups and the molecular skeleton, which allows the approach of two monomers and the formation of the cyclic dimers **17**. This steric interaction is absent in **26** and repulsion between aryl protons of two different monomers hinder the cyclic dimer formation. However, **26** can form hydrogen bonds with bases B such as trimethylamine, which catalyze the intramolecular proton transfer from one nitrogen to the other in the complex **27**.

By contrast, this process is slow as compared to hydrogen bond exchange. In other words, in each tautomerization another base molecule always carries the same proton back and forth without intermolecular proton exchange. **27** is stable only at low temperatures, but dissociates at higher temperatures. Thus at low

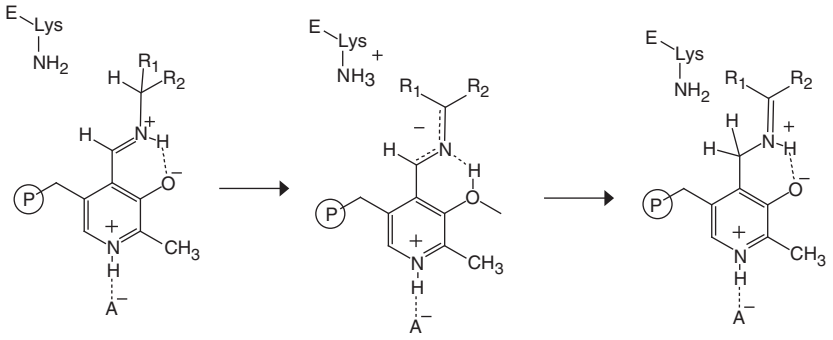

Figure 14.11 Lysine 258 catalyzed 1,3-prototropic shift of the central intermediates in the transamination reaction between the external and the internal aldimine of aspartate aminotransferase. (Adapted from [53].)

temperatures the pre-equilibrium does not play a role, whereas at high temperatures the reactants must first meet again for the tautomerization to occur. This leads to a convex slope of the Arrhenius curves [51].

Semi-empirical calculations showed a highly polar or even zwitterionic transition state which might involve some solvent reorganization. However, this may take place only temporarily, but not between the reactant and product.

Let us point out here an interesting connection of the role of lysine 258 in aspartate aminotransferase in a study conducted by Toney *et al.* [53]. The enzyme activity was strongly reduced by changing this lysine residue by alanine, a result attributed to an 1,3-prototropic shift catalyzed by the lysine amino group as illustrated in Figure 14.11. In a similar way as in the case of **26** a proton is transferred from carbon to the amino group which performs a small motion and delivers the proton back to the adjacent carbon. This type of catalysis is very different from the one in aqueous solution where the main action would be to increase the pH. We will come back to this enzyme in a later section when we discuss the role of strong hydrogen bonds on complex tautomerizations.

14.3.4
Mechanisms of Tautomerizations without Requiring Reorganization of the Environment

In some of the systems discussed in the previous sections it was found that the degeneracy of the tautomerizations is lifted by going from the gas phase to the condensed phases. An important question is then how the potential wells of tautomeric processes are influenced by the environment. Based on solid state NMR studies of azaannulenes **8** a scenario was developed [54], which is illustrated schematically in Figure 14.12. The scenario describes the fate of the potential curves of a bistable molecule exhibiting a symmetric double well for the proton motion in the gas phase after placing the molecule in condensed matter.

When the molecule is placed in a molecular crystalline environment, the crystal field will induce an energy difference ΔE between the two tautomers. ΔE will be

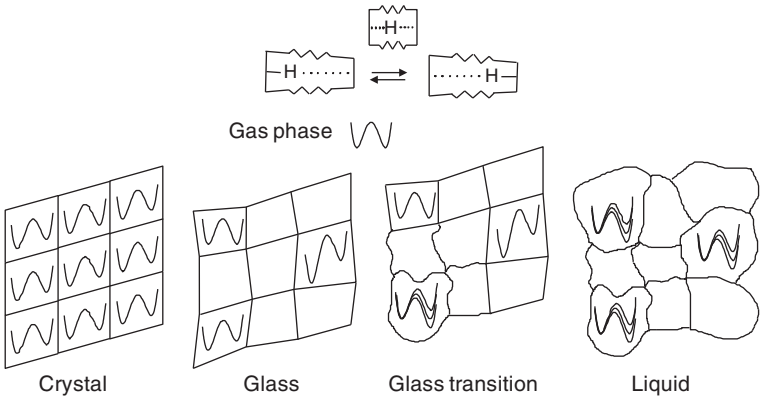

Figure 14.12 Perturbation of a double minimum potential of a bistable molecule by intermolecular interactions (Reproduced from Wehrle *et al.* [54]. Copyright (1988), with permission of American Chemical Society.). The symmetric double minimum potential in the gas phase is lifted in condensed phases. In the crystalline state all molecules experience the same perturbation, that is, the same energy difference between the two minima if strong intermolecular interactions are absent. In a glass the molecules are perturbed in a different way. At the glass point a coexistence of glassy rigid and liquid mobile environments is observed. In the latter, fast averaging of the asymmetric double wells occurs restoring a degenerate proton transfer in long time scales.

the same for all molecules in a crystal – assuming absence of a coupling of proton transfers in adjacent molecules – whereas ΔE will depend in a disordered system such as a glass on the local environment, leading to a distribution of ΔE-values. At the glass point, some environments may become mobile leading to an average value of $\Delta E_{\mathrm{av}} = 0$, whereas other environments still experience nonzero values. Only well above the glass transition a situation typical for the liquid is reached where all molecules exhibit an average value $\Delta E_{\mathrm{av}} = 0$.

An important consequence of the hydrogen bond correlations is that the barriers of H-transfer strongly depend on the energy necessary to compress the hydrogen bonds. These energies are often larger for intramolecular H-transfers as compared to intermolecular transfers. Figure 14.13 summarizes the findings schematically [4]. Figure 14.13a illustrates hydrogen bond compression during a single H transfer process according to the hydrogen bond correlation of Figure 14.1. In the initial and final states, the substitution of H for D implies a shortening of the covalent bond distance and a lengthening of the hydrogen bond [3]. In the transition state the deuterated system will be somewhat more compressed as compared to the protonated system, because the wave function of D is sharper than the wave function of H, that is, D is closer to the H-bond center than H. The barrier height is larger for D than for H.

The mechanism of a double hydrogen transfer (HH transfer) depends on whether the two hydrogen bonds involved are cooperative (Figure 14.13b) or anticooperative (Figure 14.13c). In the case of two cooperative hydrogen bonds the compression of one bond leads also to a compression of the second bond. Compression of one of two anticooperative bonds leads, however, to

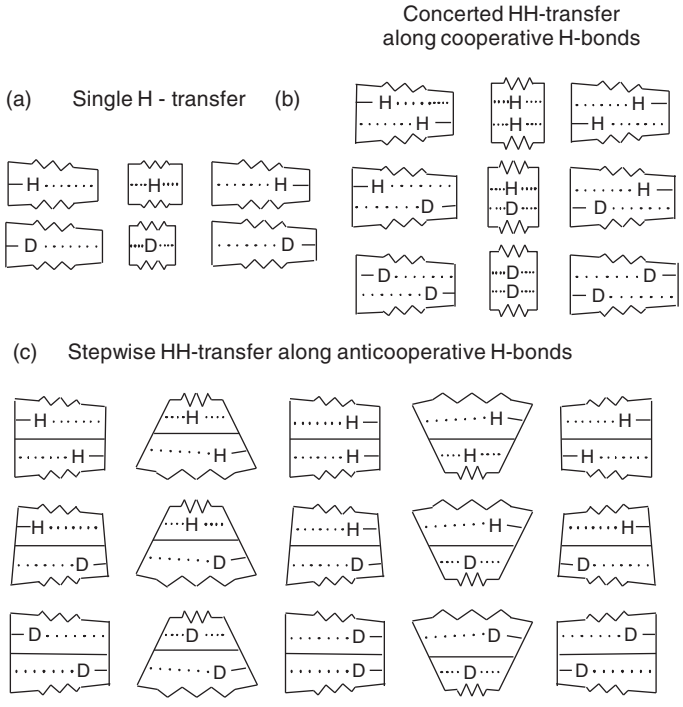

Figure 14.13 Simplified models of H- and D-substituted hydrogen transfer systems (Reproduced from Limbach [4]. Copyright (2007), with permission of Wiley.). The boxes containing springs symbolize the symmetries and the compressibilities of the hydrogen bonds. (a) Geometric H/D isotope effects during compression assisted H transfer in a single hydrogen bond. (b) Geometric H/D isotope effects during compression assisted concerted HH transfer in two cooperatively coupled hydrogen bonds. (c) Geometric H/D isotope effects during compression assisted stepwise HH transfer in two anticooperatively coupled hydrogen bonds.

a lengthening of the other bond. Thus, only a single H is transferred leading to a stepwise motion involving a metastable intermediate. Similar considerations can be made also for multiple HHH or HHHH transfers [4].

14.3.5
An Application to the Function of the Imidazole Ring of Histidine 64 in Human Carbonic Anhydrase II

While pyrazoles exhibit a molecular structure which enables the formation of cyclic hydrogen-bonded complexes in which multiple proton transfer can take place (see Figures 14.8 and 14.9), the related imidazoles exhibit a much more complex behavior. However, imidazole constitutes the functional group of histidine, which is essential to protein structure and function.

This is, in particular, the case for human carbonic anhydrase II (HCA II) [55]. The enzyme catalyzes the hydration of CO_2 as well as the backward reaction and

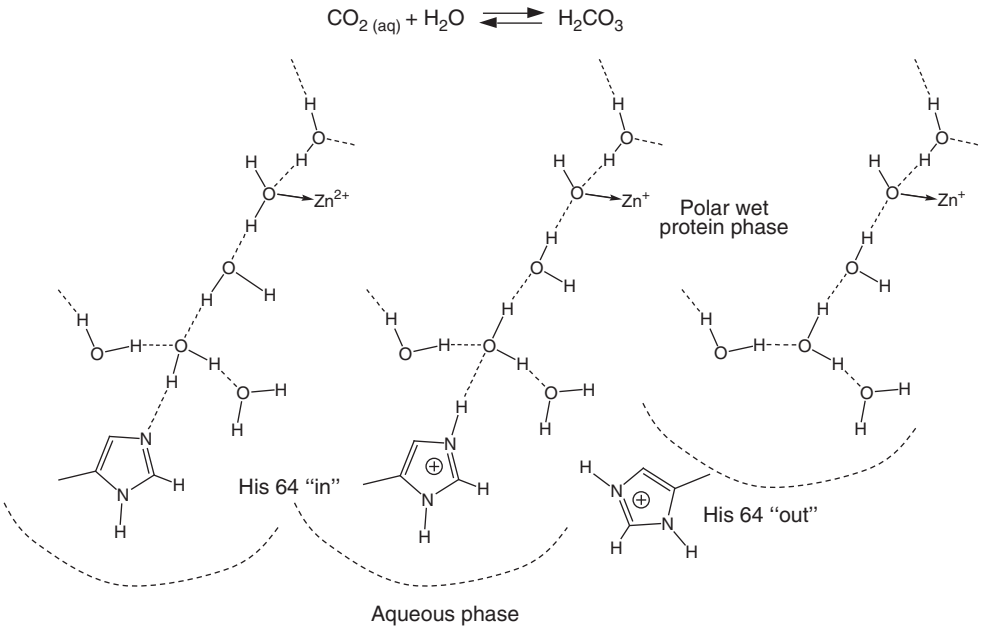

Figure 14.14 Multiple proton transfer from zinc-bound water of human carbonic anhydrase II to the imidazole ring of histidine 64. The latter is located in an inward position but moves after protonation to an outward position where it delivers the proton to the aqueous phase. The curved dashed line indicates the boundaries between the aqueous phase and the active site. (Adapted from [13].)

exhibits a zinc cation as essential cofactor. The rate-limiting step has been found to be a multiple proton transfer from Zn-bound water to the imidazole ring of histidine 64 located in the enzyme active site in an inward position as illustrated in Figure 14.14. The phase boundaries between the active site and the aqueous phase are symbolized in Figure 14.14 by curved dashed lines. When histidine 64 becomes protonated it performs a conformational change into an outward position where it delivers the excess proton to the aqueous phase [56]. Eventually, histidine 64 returns to the inward position until the cycle starts again.

Recently, Shimahara *et al.* [57] observed a very interesting behavior of histidine 64 in HCA II. Usually, as illustrated in Figure 14.15a, imidazole rings of histidines are located in protein surfaces sticking into water exhibit a large equilibrium constant K_t of tautomerism, that is, the proton is preferentially bound to N-1 forming the τ-tautomer. The π-tautomer where the proton is bound to N-3 is non-dominant.

Using ^{15}N NMR a very different result was observed for the imidazole ring of histidine 64 in the active site of HCA II. The imidazole was subject to a fast tautomerism, but K_t was found to be unity within the margin of error as illustrated in Figure 14.15b. This difference could not be explained in a satisfactory way.

However, recently Shenderovich *et al.* [13] showed using ^{15}N NMR studies performed on 4-methylimidazole dissolved in a CDF_3/CDF_2Cl solvent mixture

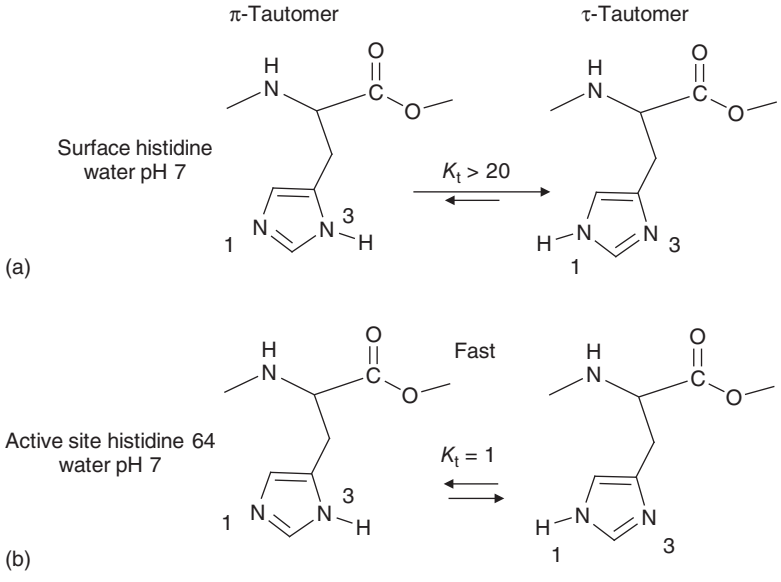

Figure 14.15 Equilibrium constants of tautomerism K_t of surface histidines (a) and histidine 64 (b) in the active site of HCA II [57].

that a value of $K_t = 1$ is typical for a wet polar aprotic environment – where some water molecules are necessary to catalyze the proton exchange – but larger values of K_t are typical for aqueous solution. In other words, neutral histidine 64 in HCA II prefers the inward position, but once it is protonated it prefers the outward position where an aqueous environment is experienced.

Figure 14.16 illustrates a possible proton exchange mechanism of the neutral histidine 64 in the active site of HCA II. As indicated by K_t, the local environment resembles a wet polar aprotic solution exhibiting a high molecular mobility, which enables the tautomerism by simple reorganization of some water molecules.

In other words, the tautomerism of histidines constitutes a molecular environmental probe. Moreover, model studies for the interior of proteins should not be made using water but wet polar organic liquids as solvents.

14.4
Tautomerizations Requiring Reorganization of the Environment

Tautomerizations requiring reorganization of the environment are most often associated with the transfer of electrical charges. Whereas molecular reorganization is hindered in the solid state it becomes important in liquid solutions and in biomolecules. Most often, strong hydrogen bond formation plays an important role. In order to study hydrogen bond properties in solution in the past decades NMR tools have been developed, which rely on correlations of NMR parameters such as chemical shifts and scalar coupling constants with hydrogen bond geometries, obtained for solids and then applied to liquids [3]. In particular, the

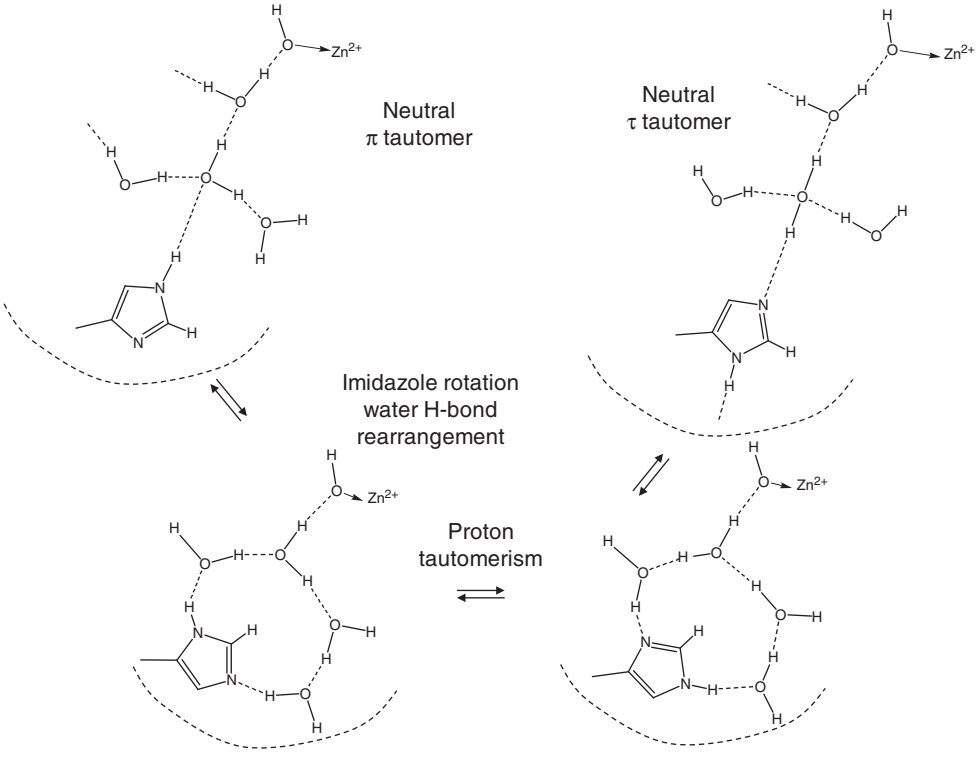

Figure 14.16 Mechanism of the tautomerism of histidine 64 in HCA II according to Shenderovich *et al.* [13].

discovery of coupling constants across hydrogen bonds has promoted this area of research. One of the important questions is the proton density distribution function along the hydrogen bond coordinate q_1. Several possibilities have been discussed previously [16], which led eventually to the development of combined UV-Vis and NMR spectroscopy of hydrogen-bonded complexes [58].

In this section, we will not describe the development of such tools but focus on examples. In the first part we will deal with tautomerizations of charged molecules and hydrogen-bonded clusters, and in the second part we will deal with neutral systems where tautomerizations lead to highly polar or zwitterionic states. The systems discussed have all been studied by NMR and were selected in view of the general molecular stories they tell us.

14.4.1
Tautomerization of Charged Molecules and Hydrogen Bonded Clusters

14.4.1.1 Proton Sponges

Let us start with the discussion of some charged and – for comparison – of some neutral systems exhibiting strong intramolecular formally symmetric NHN

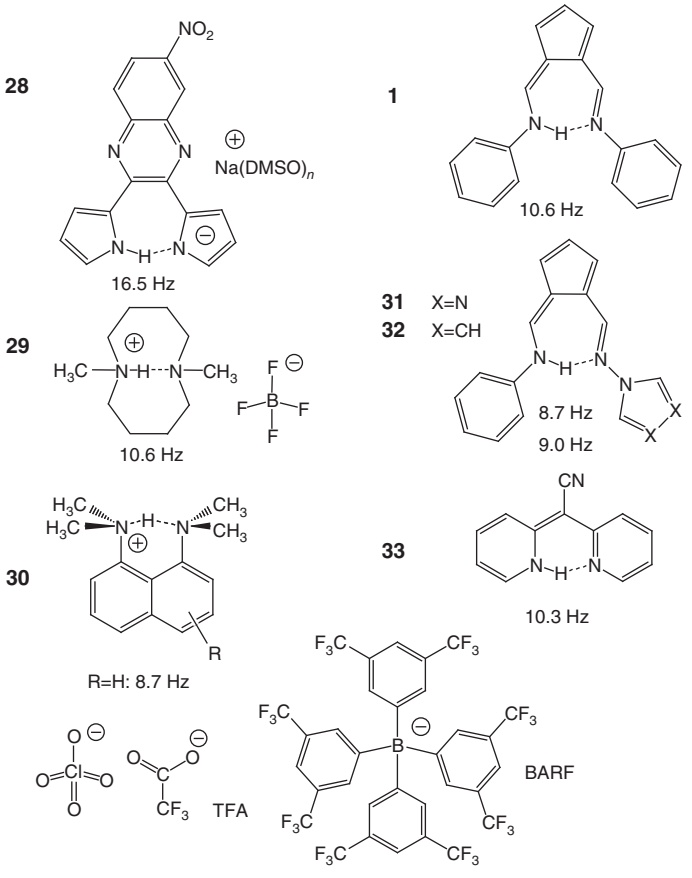

Figure 14.17 ^{15}N labeled systems exhibiting strong intramolecular NHN hydrogen bonds. **28**: deprotonated mono-anion of 6-nitro-2,3-dipyrrol-2-ylquinoxaline [59]. **29**: protonated mono-cation of 1,6-dimethyl-1,6-diazacyclodecane [59] and **30** of 1,8-bis(dimethylamino)-naphthalene (DMAN, proton sponge) [60]. For comparison, the neutral molecules *N*,*N*′-diphenyl-6-aminopentafulvene-1-aldimine (**1**, see Figure 14.3), *N*-phenyl-*N*′-(1,3,4-triazol)-6-aminopentafulvene-1-aldimine (**31**), *N*-phenyl-*N*′-(pyrrol)-6-aminopentafulvene-1-aldimine-(**32**), bis-(2-pyridyl)-acetonitrile (**33**) are also depicted. (Adapted from [60].) The numbers in Hz indicate the scalar couplings J_{NN} across the intramolecular hydrogen bond. TFA^-: trifluoroacetate, $BARF^-$: tetrakis[3,5-bis(trifluoromethyl)phenyl]borate.

hydrogen bonds (Figure 14.17). The hydrogen bond strength is manifested by the finding of large proton chemical shifts above 19 ppm, large H/D isotope effects on the latter, and of large coupling constants J_{NN} across the NHN hydrogen bond. Generally, CD_2Cl_2 was used as solvent. In the case of the anion **28** the counter cation Na^+ was solubilized by addition of some DMSO-d_6 [59]. In a study of the cations **29** and **30** the counter anion BF_4^- was used [61]. **30** and substituted derivatives were studied using varying counter anions, for example, ClO_4^-,

trifluoroacetate (TFA^-) and tetrakis[3,5-bis(trifluoromethyl)phenyl]borate ($BARF^-$) [60].

It is noteworthy that for the neutral systems **1**, **31**, **32**, **33** in Figure 14.17 and the anion **28** the coupling constants J_{NN} correlate well with the proton chemical shifts, indicating that both quantities are good measures for the strength of the corresponding hydrogen bonds. Moreover, **28** is the system with the largest value (16.5 Hz) found up to date. The values of J_{NN} are smaller for the proton sponges **29** and **30** because of the different nitrogen hybridization.

The main point here is the finding that the anion **28** is not much affected by counter cation, solvent, and temperature changes; that is, it behaves in a similar way as the neutral systems in Figure 14.17 (**1**, **31**, **32**, **33**). This can be associated with the extended charge distribution in **28**.

By contrast, the charge is much more localized in proton sponges such as **29** and **30**. Both, the smaller strongly interacting BF_4^- and the larger noncoordinating anion $BARF^-$ were used as anions in the case of **30**. The NMR parameters depended substantially on solvent, temperature, and on the counter anion [60]. A scenario arising from these studies is depicted in Figure 14.18.

Figure 14.18a deals with the case of the dissociated ion pair as found for acetonitrile. At room temperature, the solvent molecules around the positively charged nitrogen atom may exhibit a higher local order parameter than those in the vicinity of the neutral nitrogen atom. This can weaken the hydrogen bond via ion–dipole interactions in both tautomers **a** and **b**. When temperature is lowered leading to an increase of solvent ordering the hydrogen bond becomes more symmetric (Figure 14.18b). This "symmetrization" is manifested by the evolution of ^1H chemical shifts and scalar coupling constants J_{NN}, J_{NH}, and J_{HN}.

Figure 14.18 also illustrates the role of the counter anion which now forms a contact or solvent separated ion pair with the cation containing an intramolecular hydrogen bond. When the anion is small (Figure 14.18c), it will again perturb the hydrogen bond symmetry and weaken it if it is placed asymmetrically [8]. By contrast, a large counteranion in which the negative charge is well delocalized will lead to a symmetrization, that is, strengthening of the hydrogen bond as depicted schematically in Figure 14.18d. Solvent reorganization at low temperatures will still play an important role.

A related result was obtained with protonated bipyridine **34** dissolved in CDF_3/CDF_2Cl [62] depicted in Figure 14.19. The intramolecular hydrogen bond of **34** is subject to some steric strain and can more easily form intermolecular hydrogen bonds as compared to proton sponges. Dichloroacetate makes a strong hydrogen bond, and takes up the proton from one nitrogen and brings it to the other nitrogen in a similar way as **27** (see Figure 14.19c). On the other hand, the hydrogen bond to BF_4^- is weaker and the intramolecular hydrogen bond in which an intramolecular tautomerization takes place can compete (Figure 14.19b). By contrast, only the noncoordinating anion $BARF^-$ as counter anion enables the preferential formation of the intramolecular hydrogen bond (Figure 14.19a).

Recently, several homoconjugated pyridine and substituted pyridine cations of type **35** (Figure 14.19d) have been studied by low-temperature NMR spectroscopy

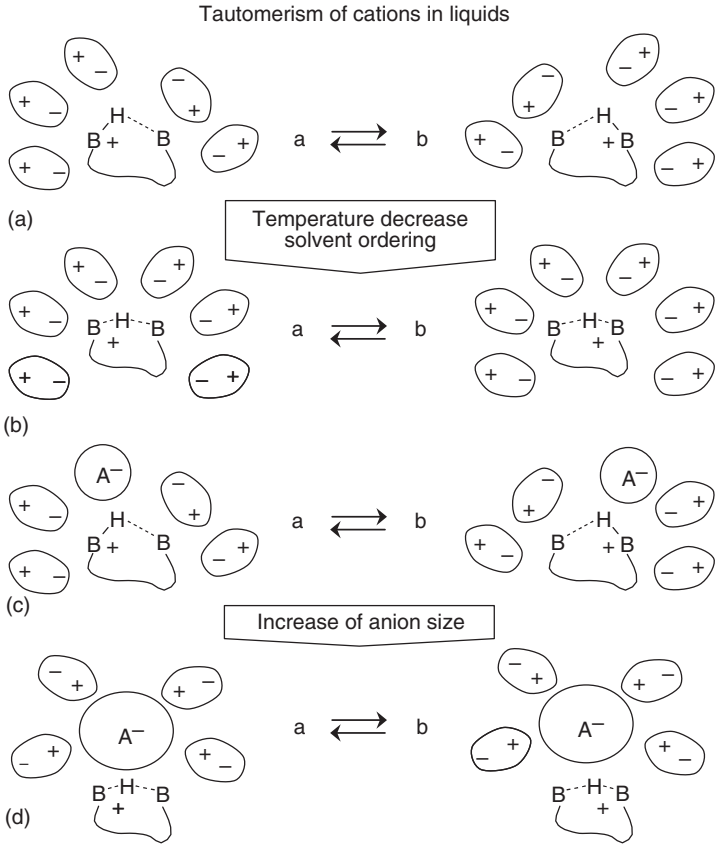

Figure 14.18 (a) Differential solvation of a homoconjugated cation at room temperature. The positively charged acceptor site containing the proton experiences a higher local solvent order than the neutral acceptor site. Tautomerism is accompanied by solvent reorganization. (b) Solvent ordering by lowering the temperature increases the symmetry of the hydrogen bond. (c) Interaction with a small counteranion which is placed in an asymmetric way with respect to the hydrogen bond weakens the hydrogen bond. (d) Interaction with a large counteranion where the positive charge is delocalized and well shielded from the solvent can symmetrize and strengthen the hydrogen bond. (Reproduced from Pietrzak *et al.* [60]. Copyright (2010), with permission of Wiley.)

(solvent CDF_3/CDF_2Cl) [63]. The NMR parameters of **35** are the same for BF_4^- and $BARF^-$, that is, the hydrogen bonds of **35** are not broken by BF_4^-. The observation of NMR high-field shifts of the hydrogen-bonded deuteron as compared to hydrogen indicate a situation as is depicted in Figure 14.2a or c, that is, with a fast tautomerism. A correlation of NMR parameters with hydrogen bond geometries indicated that the shortest N···N distance is about 2.65 Å. *ortho*-Substituents prevent N···N distances shorter than 2.7 Å. Note that to our knowledge the shortest known N···N distance of intermolecular NHN hydrogen bonds is about 2.54 Å [8].

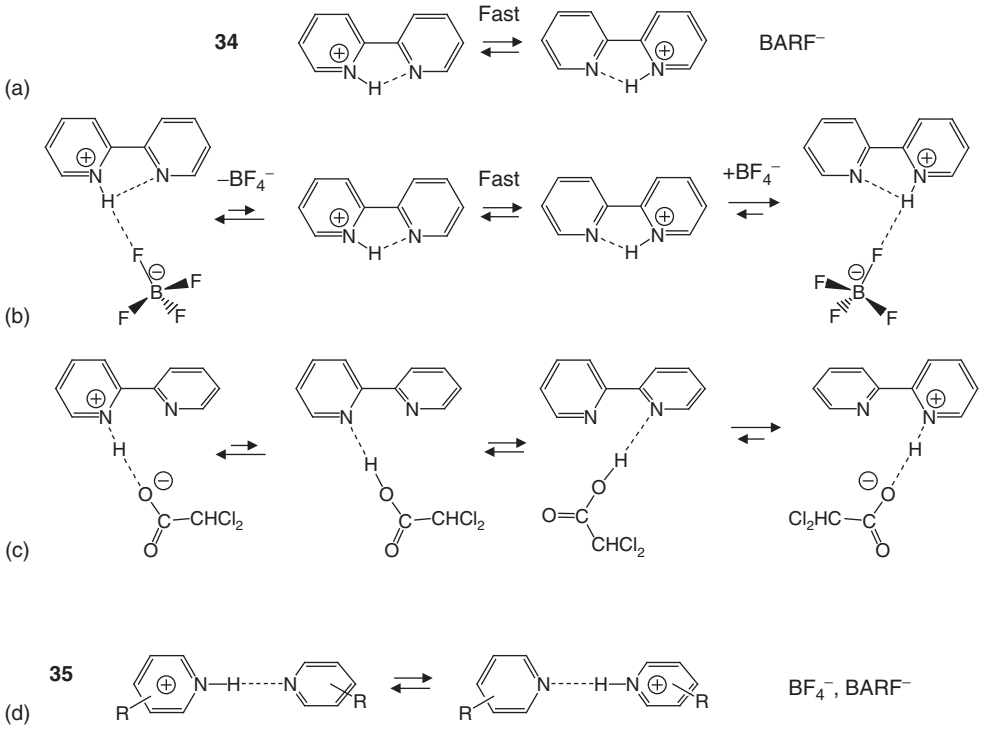

Figure 14.19 (a–c) Counteranion-dependent hydrogen bonding and proton tautomerism of protonated bipyridine **34** dissolved in CDF_3/CDF_2Cl. (Adapted from [62].) (d) Proton tautomerism of the protonated pyridine dimer **35** according to [63, 64].

A recent IR spectroscopic study (solvent CD_2Cl_2) indicated different vibrations for the pyridine and the pyridinium moiety [64]. The exchange rate was estimated to be between 10^6 and 10^{11} s^{-1}.

14.4.1.2 Phenol–Carboxylate versus Carboxylic Acid–Phenolate Complexes

Acid–base hydrogen bonds between phenol- and carboxylate moieties occur often in biomolecules. An example is the photoactive yellow protein (PYP) depicted in Figure 14.20. A neutron crystallographic study revealed a strong hydrogen bond between the cofactor *p*-coumaric acid thioester and the carboxylate group of glutamic acid 46, and a weaker one between tyrosine 42 and the cofactor [65]. Interestingly, the proton was found to be located closer to the carboxylate oxygen than to the phenolic oxygen. PYP reacts to light irradiation and the initial elementary step is considered to be a proton transfer along the hydrogen-bonded chain.

In order to understand this interaction as well as a potential tautomerism of these systems, various simplified model systems of the type AHX^- (**36** in Figure 14.21) were generated from mixtures of substituted phenols (AH) with tetra-butylammonium carboxylates (X^-) in polar organic solvents such as CD_2Cl_2

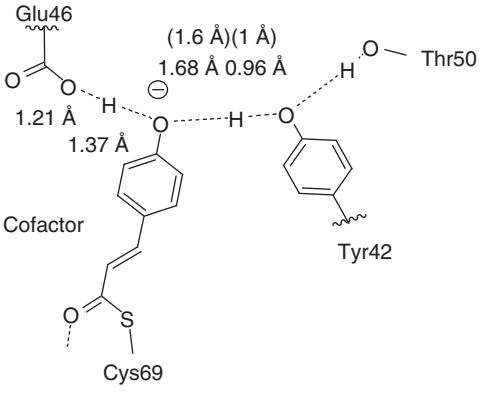

Figure 14.20 Neutron crystallographic structure of the photoactive yellow protein (PYP) [65].

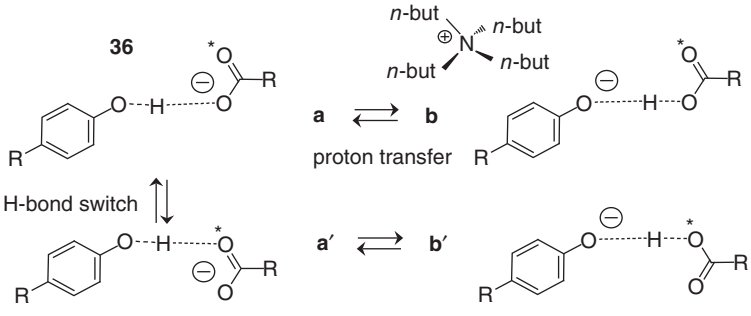

Figure 14.21 Proton transfer and hydrogen bond switch in phenol-carboxylate/phenolate/carboxylic acid complexes **36** as PYP model systems. Counter cation: tetrabutylammonium.

or CDF_3/CDF_2Cl. These model systems have been studied by a combination of UV/Vis and NMR spectroscopy [58, 66, 67] where both spectroscopies were applied at the same time at low temperatures. In the visible range, only the phenolic moieties give rise to the UV/Vis spectra. Low temperatures were required to reach the slow hydrogen bond exchange regime.

The question studied was the problem of whether there is a tautomerization, that is, proton transfer between two tautomers **a** and **b** (situations *iii* to *v* in Figure 14.1) or whether there is a series of asymmetric low-barrier hydrogen bonds (*vi* in Figure 14.1) as was illustrated in Figure 14.2. In addition, we note that fast hydrogen bond switches can occur, which effectively transfer the proton between the two oxygen atoms as illustrated in Figure 14.21. This process corresponds formally to the IUPAC definition. We will come back to this question in the next section.

In a first step, it was possible to identify the NMR parameters and UV/Vis bands of the complexes AHX^- of interest. Both single as well as dual UV/Vis absorption

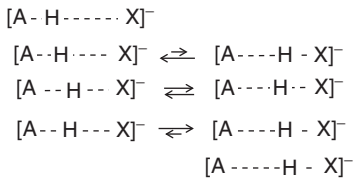

Figure 14.22 Proton transfer configurations of nonsymmetric OHO hydrogen bonds.

bands were observed, depending on the molecular structure, solvent, and temperature. Using ^{1}H and ^{13}C NMR of the partially deuterated complexes it was possible to assign the systems with single bands either to tautomers of type **a** or type **b**. Using ^{1}H chemical shift correlations of OHO hydrogen bonds [5] the hydrogen bond coordinates q_1 and q_2 were obtained and a correlation of the latter with the UV/Vis band frequencies was established. From the band intensities the equilibrium constants of the tautomerism were estimated.

In the case of weaker hydrogen bonds only single tautomers are observed (*ii* and *vii* in Figure 14.1), whereas two tautomers were observed for the stronger hydrogen bonds. It was found that the dominant tautomer exhibited the weaker and the nondominant tautomer the stronger hydrogen bond (*iii* to *v* in Figure 14.1). The situation is expressed qualitatively in a more traditional way in Figure 14.22. Unfortunately, the hydrogen bond switch depicted in Figure 14.21 could not directly be verified, although such switches were found in related anions as described in the next section.

Pylaeva *et al*. [68] have recently performed *ab initio* molecular dynamics calculations of the 4-nitrophenol-acetate complex **37** in a solvent box containing 70 CD_2Cl_2 molecules at a temperature of 300 K. Figure 14.23a illustrates the hydrogen bond geometries q_2 versus q_1 sampled during the simulation. It shows that not only two tautomers with well-defined q_2 and q_1 values are formed but a broad distribution of tautomers with different geometries are also observed, including quasi-symmetric configurations with values around $q_1 = 0$.

Figure 14.23b depicts the overall proton position distribution. Again, the obtained distribution is very broad; it covers the range from quasi-symmetric hydrogen bonds to highly asymmetric hydrogen bonds; structures interconvert due to the solvent motions. In the presence of the counter cation there are two broad maxima corresponding roughly to tautomers **a** ($PhOH\cdots OAc^-$) and **b** ($PhO^-\cdots HOAc$). Interestingly, **b** seems to dominate although it is well known that 4-nitrophenol is less acidic (pK_a 7.1, [69]) than acetic acid (pK_a 4.75 [70]). Without the countercation, the effect is even enhanced, as illustrated in Figure 14.23b; here almost only the tautomer **b** ($PhO^-\cdots HOAc$) is found.

It follows that the geometries represented in a correlation diagram such as Figure 14.1 represent average geometries corresponding to the maximum of the distribution peaks in Figure 14.23. In other words, when discussing correlation diagrams one must consider that distributions of hydrogen bond geometries are neglected.

The finding that in a heteroconjugated anion embedded in a polar environment phenols transfer the proton to the carboxylates is rationalized schematically in

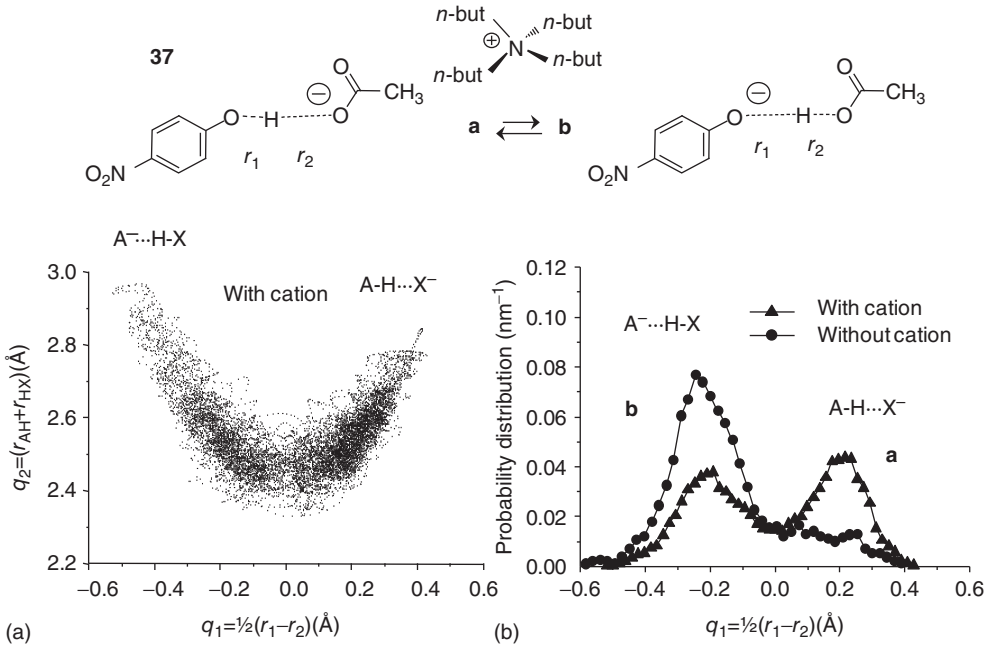

Figure 14.23 Results of *ab initio* molecular dynamics simulations of **37** in CD_2Cl_2 at 300 K (Reproduced from Pylaeva *et al.* [68]. Copyright (2015), with permission of Royal Society of Chemistry.). (a) Set of hydrogen bond geometries q_2 versus q_1 sampled during the trajectory simulation in the presence of the counter cation. (b) q_1 distribution for the trajectory with (triangles) and without the counter cation (circles).

Figure 14.24. In an unpolar environment, in the presence of weak interactions with a countercation, the charge prefers the residue exhibiting the higher electron delocalization, that is, the phenol moiety and hence the proton is located near a carboxylic oxygen. By contrast, in a very polar environment the Coulomb interactions stabilize the configuration with the smaller distance between the positive and negative charges, hence the carboxylate is preferred [67]. Furthermore, we note that weak hydrogen bonds formed between the carbon–hydrogen groups of the solvent with the "free" C═O group of the carboxylate lead to a distribution of the geometries of the OHO hydrogen bonds and of the complex conformations [68].

14.4.1.3 **Homoconjugated Carboxylic Acid Carboxylates**

In solutions of tetra-butylammonium acetate with additional acetic acid using CDF_3/CDF_2Cl as a solvent for low-temperature NMR studies in the slow hydrogen bond exchange regime below 150 K various complexes of the type $Ac^-(HAc)_n$, $n = 1,2,3$ have been observed [71] as depicted in Figure 14.25. All complexes showed H/D isotope effects on ^1H, ^2H, and ^{13}C chemical shifts, which let one to identify the different complexes and indicate the presence of strong hydrogen bonds. While for the homoconjugate anion or hydrogen diacetate **38** a very fast degenerate proton transfer was expected averaging the carbon chemical

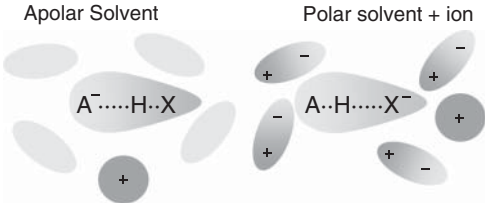

Figure 14.24 Schematic representation of solvation effects on the hydrogen bond geometries of heteroconjugated anions. In an apolar environment, in the presence of weak interactions with a countercation, the charge prefers the residue exhibiting the higher electron delocalization. Polar environments and the presence of the countercation drive proton transfer in the sense that the charge becomes more localized. (Reproduced from Koeppe *et al.* [67]. Copyright (2013), with permission of American Chemical Society.)

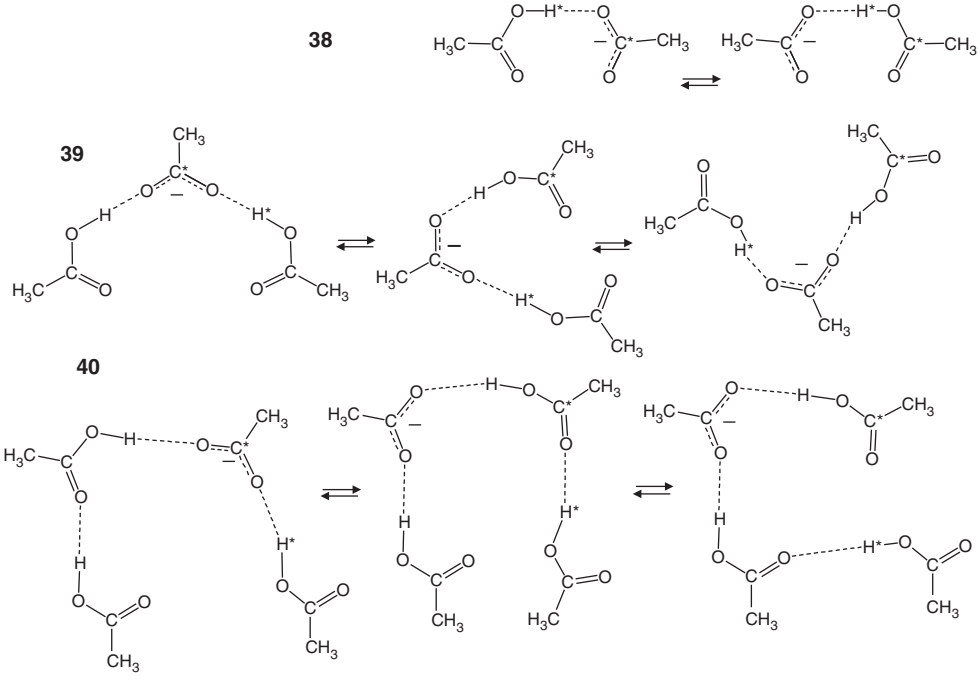

Figure 14.25 Chemical structures and fluxionality of hydrogen diacetate **38**, dihydrogen triacetate **39,** and trihydrogen tetraacetate **40** according to [71].

shifts, that was not expected for the other two complexes, dihydrogen triacetate **39** and trihydrogen tetraacetate **40**. The latter exhibited an interesting fluxionality in the sense that all carboxylic acid moieties became equivalent. These processes involve a series of hydrogen bond switches of one of the outer carboxylic acids to the other outer carboxylic acid followed by a proton transfer. This establishes the central moieties as carriers of the negative charges. Thus, at the end, all carbon atoms and also all oxygen atoms become equivalent. Again, one can describe part

of these processes in terms of a traditional tautomerization, that is, of proton transfer from one carboxylic acid oxygen to the other.

Similar results have been obtained for homoconjugated anions of other carboxylic acids (inter- [72] and intramolecular [73]) and trimethylglycine TFA [74].

14.4.2 Tautomerization of Neutral Heterocyclic Acid–Base Complexes

The characteristics of the tautomerization of neutral molecules along intramolecular hydrogen bonds are different from the charged complexes although some features are similar. The normal tautomer of a neutral system exhibits a relatively small dipole moment but exhibits a large one in a zwitterionic state formed by proton transfer. Naturally, this requires again larger solvent reorganization; the difference with the charged systems is only that a counterion is absent.

14.4.2.1 Model Complexes of the Acid–Pyridine Type

Hydrogen-bonded complexes of inorganic and organic acids with heterocyclic bases have been of great interest in view of their biological importance in proteins. Most often, substituted pyridines have been studied as heterocyclic bases. Here, we focus on results obtained by solid state and liquid state NMR.

Complexes of 2,4,6-trimethylpyridine (collidine) with HF dissolved in CDF_3/CDF_2Cl down to 100 K are depicted in Figure 14.26. The different complexes **41**–**44** formed could be characterized in the slow hydrogen bond exchange

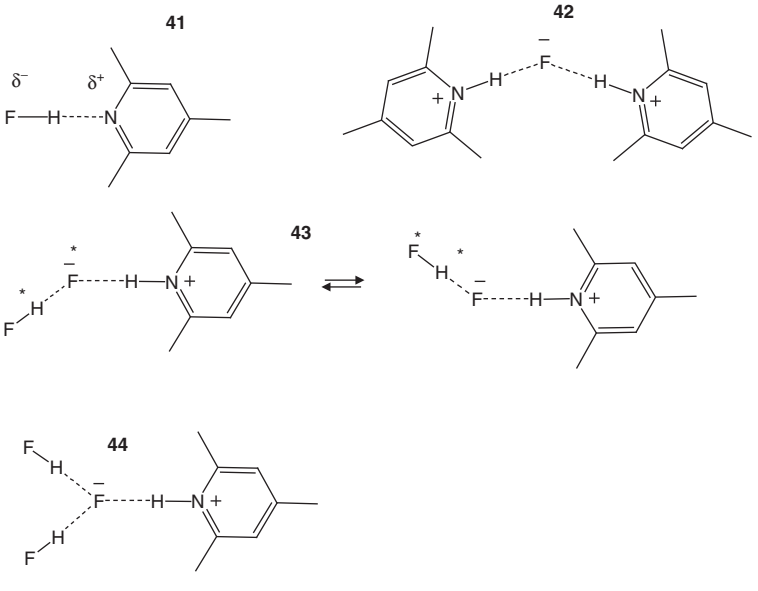

Figure 14.26 Chemical structures and fluxionality of collidine–HF complexes according to [75].

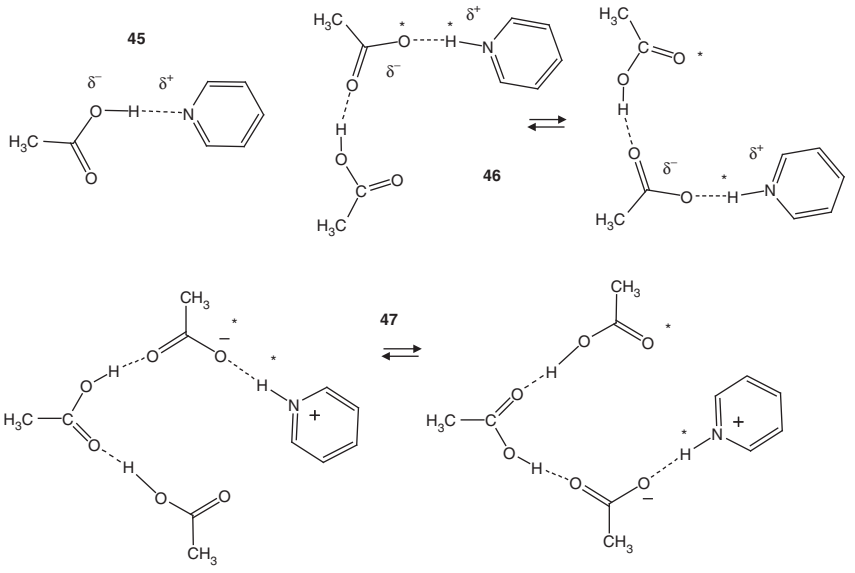

Figure 14.27 Chemical structures and fluxionality of pyridine–acetic acid complexes according to [15].

regime by multinuclear NMR [75, 76]. Noteworthy was the discovery of scalar couplings across the FHN–hydrogen bonds, that is, between all nuclei of the $^{19}F-^{1}H-^{15}N$ system. For **41,** major coupling constant changes occurred when lowering the temperature indicating a transformation from a molecular to a zwitterionic complex. In order to understand these effects, the dielectric constant ε of the solvent mixture was measured down to 100 K [77]. While ε was smaller than 10 at room temperature it increased to about 45 at 100 K. **43** exhibited a very fast hydrogen bond switch within the complex. If H would be located closer to fluorine than to nitrogen it would correspond to the IUPAC definition of tautomerism.

Similar results were obtained for pyridine–acid complexes such as shown in Figure 14.27 [15, 78]. In the 1 : 1 complex **45** at low temperatures, H was located closer to oxygen, shifted toward the H-bond center for **46** and became zwitterionic for the **47**. For the latter, the hydrogen bond switch could be established, which is, probably, also present in **46**. H/D isotope effects on NMR chemical shifts gave information about average structures, in particular how the geometry of a given hydrogen bond changes when the adjacent bond is deuterated.

Figure 14.28 summarizes the main results. When the polarity of the environment of an acid–base complex is increased the dipole moment of a AHB complex is increased. For a molecular complex that realized by charge transfer from the base to the acid, leads to a shortening of the A···B distance and to a shift of the proton toward the hydrogen bond center as described by the correlation curve in Figure 14.1 [16]. Once H has passed the hydrogen bond center the dipole

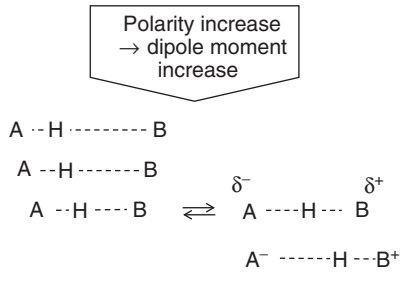

Figure 14.28 Proton transfer configurations of OHN hydrogen bonds converted from neutral to zwitterionic by an increase of the polarity of the environment.

moment is increased by an increase of the A···B distance [16]. As ε increases with decreasing temperature, the molecular complex becomes stronger and a zwitterionic complex such as the pyridine–HCl complex becomes weaker. We note that in the solid state ε is small, and therefore large solid–liquid effects on the hydrogen bond geometries are observed because of the polarity increase that occurs when the systems are taken out from the solid to polar solution [79]. Specific solvation by additional acid molecules can have similar effects as nonspecific solvation obtained by an increase of ε. This is especially important in proteins. An anti-parallel arrangement of two polar OHN hydrogen bonds can then lead to zwitterionic states [11].

By measuring and analyzing H/D isotope effects on ^{13}C chemical shifts of acid–heterocyclic base complexes it was shown [80] that for very strong hydrogen bonds there is a tautomerization according to Figure 14.4a or c, as illustrated in the center of Figure 14.28. Because of the larger asymmetry of OHN as compared to the OHO hydrogen bonds the phenomenon is confined to a smaller range of q_1 values. This phenomenon does also show up in $^{1}H-^{15}N$ chemical shift correlations of pyridine–acid complexes, which indicates that the shortest O···N hydrogen bond distances which are conceivable are not reached [81].

14.4.2.2 **Mannich Bases**

Mannich bases **48** (Figure 14.29) represent interesting intramolecular models for acid–base hydrogen bonds. Their examples illustrate again the importance of an analysis using different spectroscopic techniques [82]. UV/Vis spectra of **48** in the polar organic solvent mixture CDF_3/CDF_2Cl down to 100 K showed dual bands which could be associated to two tautomeric forms, a normal one where the proton is close to the phenolic oxygen dominating at high temperatures and the zwitterionic one where the proton is close to the aliphatic nitrogen dominating at low temperatures. It was tempting to attribute this finding to a stabilization of the zwitterionic form by the solvent whose dielectric constant increases strongly at low temperatures [77]. However, related NMR experiments performed at 140 K indicated the formation of a zwitterionic dimer in which the protons are located close to nitrogen. Thus, the tautomeric equilibrium was coupled to the dimerization. Also, it was found that addition of methanol (AH) to the monomer also shifted the proton away from oxygen toward nitrogen. We will show later that this effect is important in biomolecules.

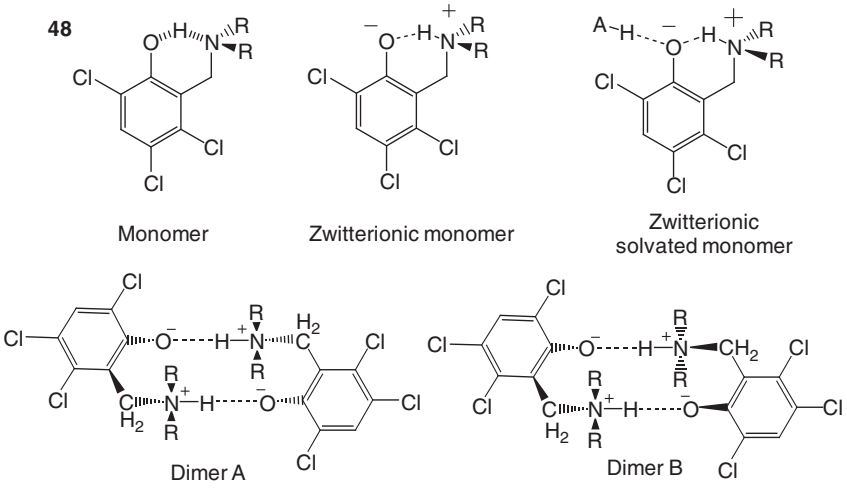

Figure 14.29 Structures of Mannich base **48** according to [82]. Dimers A and B exhibit a different stereoisomerism.

14.4.2.3 **Model Schiff Bases**

For a long time, Schiff bases have fascinated physical chemists because of their model character for proton transfer and hydrogen bonding [83]. A combined variable temperature ^{1}H and ^{15}N NMR study of the ^{15}N labeled Schiff base **49** (Figure 14.30) as well as its partially deuterated isotopologs dissolved in different organic solvents indicated a complex tautomerism [84]. The situation resembled qualitatively the one described in Figure 14.1. In polar solution, the OH· · ·N hydrogen bond of the enolimine tautomer became stronger when temperature was decreased, whereas the O· · ·HN hydrogen bond of the ketoamine tautomer became weaker; both geometric changes are, however, associated with a dipole moment increase. Thus, at high temperatures the tautomerism was characterized by situation *iii* whereas at low temperatures it was characterized by *v* as depicted in Figure 14.1. Again, this indicates a much more complex process as suggested by just the presence of an enolimine and a ketoamine structure. We note that in case of an aromatic substituent on the Schiff base nitrogen the enolimine structure dominates in view of the reduced basicity of the nitrogen.

When methanol or a fluorinated alcohol was added, hydrogen bonding to the phenolic oxygen shifted the equilibrium toward ketoamine structures. By contrast, addition of trifluoroacetic acid led to protonated **49**, forming presumably a heterodimer as illustrated in Figure 14.30. H/D isotope effects on ^{15}N chemical shifts were observed which could be dissected into intrinsic isotope effects arising from geometric isotope effects and those arising from different zero-point vibrations in the two exchanging tautomers. However, a detailed description is beyond the scope of this overview.

The effect of a covalently linked carboxylic group on the Schiff base tautomerism has been studied using the ^{15}N labeled model system **50** dissolved in CD_2Cl_2

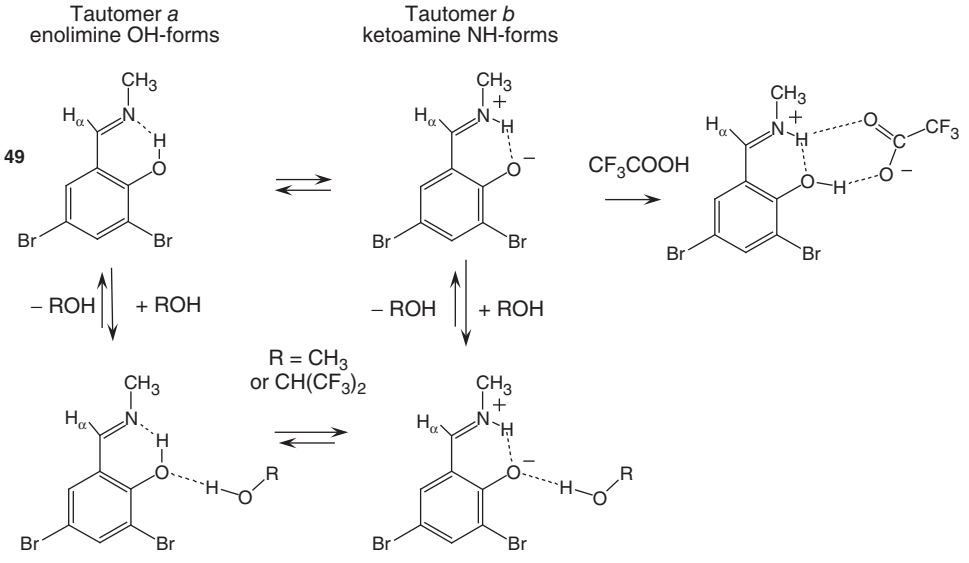

Figure 14.30 Tautomerism and protonation of the model Schiff base **49** according to [84].

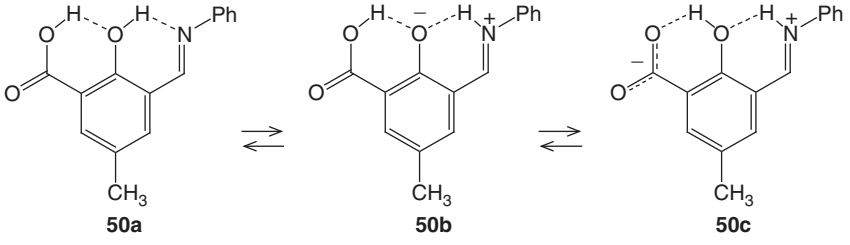

Figure 14.31 Effect of an intramolecular hydrogen bond to a carboxylic group on the tautomerism of a model Schiff base according to [85].

(Figure 14.31). All three forms could be observed, although in fast exchange [85]. The NMR parameter analysis indicated that at high temperature **50a** dominates, **50b** at intermediate temperatures and **50c** at low temperatures as expected from the increase of the solvent dielectric constants [77].

14.4.2.4 The Cofactor Pyridoxal 5′-phosphate: from Organic Models to Alanine Racemase and Aspartate Aminotransferase

Pyridoxal 5′-phosphate (PLP, Figure 14.32) is a cofactor of enzymes that are responsible for amino acids transformations such as racemization, transamination, and decarboxylation. Its enzymology has been reviewed recently [86, 87]. When PLP is embedded in an enzyme it usually forms the so-called "internal aldimine" with the ε-group of a lysine residue in the active site, or an "external aldimine" with amino acid substrates or inhibitors. The similarity with the Schiff

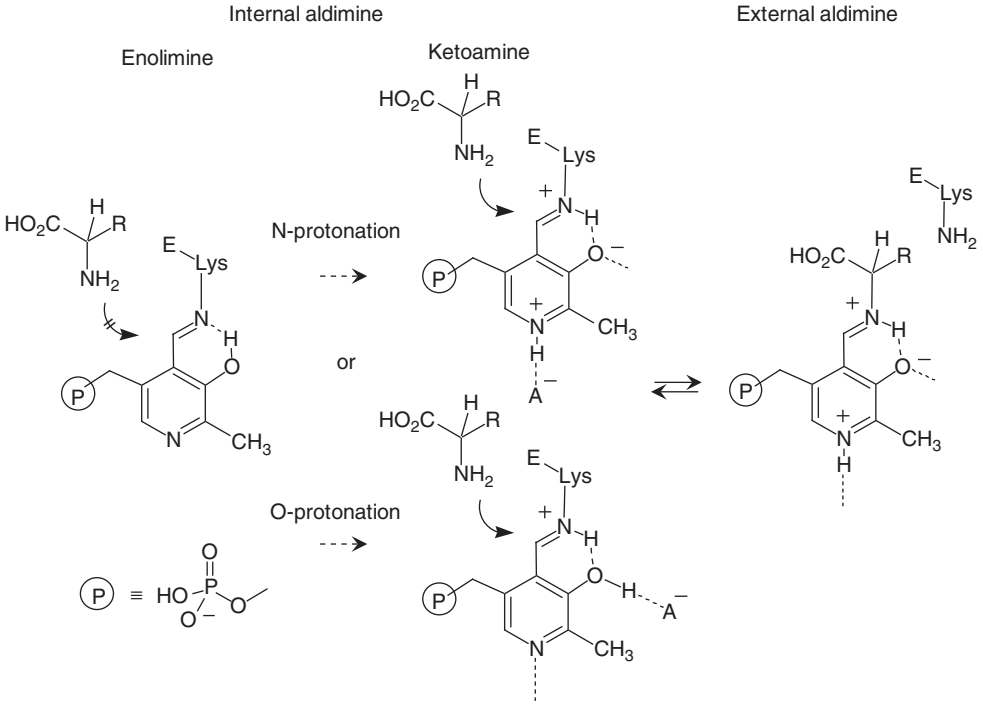

Figure 14.32 Activation of the internal aldimine of PLP for transimination between the internal and external aldimine leading to the formation of the ketoamine tautomer. Upper pathway: N-protonation, lower pathway: O-protonation.

bases described in the previous section is that these aldimines contain the same intramolecular OHN hydrogen bond in which an enolimine–ketoamine tautomerism can take place, which seems then to be an important element of the enzyme function.

As illustrated in Figure 14.32, the first step of all PLP-dependent enzyme reactions is the replacement of the lysine residue with the amino group of an incoming amino acid substrate producing an external aldimine. This reaction is called *transimination*. It has been argued that the nucleophilic attack in the first step of the latter reaction requires a positive charge on the Schiff base imino nitrogen [88–91]. For this, the bridging proton of the intramolecular OHN hydrogen bond has to be transferred from the phenolic oxygen to the imino nitrogen. Thus, the tautomerism of PLP is governed in enzyme environments by intermolecular interactions.

It has further been argued that the ketoamine is produced by protonation of the pyridine ring as illustrated in the upper part of Figure 14.32. In the lower part an alternative activation is proposed as discussed later.

Indeed, the X-ray crystal structure of *Escherichia coli* aspartate aminotransferase, in which PLP is covalently bound to Lys258 as an internal aldimine in

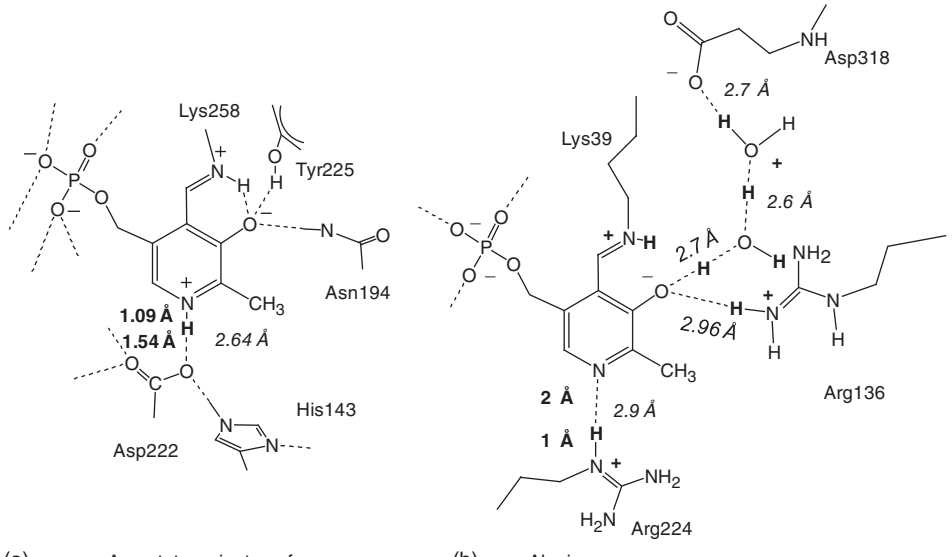

Figure 14.33 Active site structures of (a) aspartate aminotransferase [92] and (b) alanine racemase [93]. Italic distance values were derived by X-ray crystallography and bold values estimated by NMR [94, 95].

the active site has identified an aspartate residue near the pyridine ring of PLP exhibiting a short O···N distance of 2.64 Å [92] as illustrated in Figure 14.33a. Throughout Figure 14.33 italic distance values were derived by X-ray crystallography and bold values estimated by NMR as described later.

However, questions remain. Thus, as aspartic acid is more acidic (pK_a 3.9 [94] than the protonated PLP pyridine ring (pK_a 5.8 [95]), it was thought that in case of a hydrogen bond between aspartate and the pyridine ring of PLP the pyridine ring should be protonated [94, 95]. But it was not explained as to why at physiological conditions pH both residues are not protonated in aqueous solution. What makes then the proton governing the PLP tautomerism going into the aspartate–pyridine hydrogen bond in the enzyme active site?

Furthermore, alanine racemase from *Bacillus anthracis* also contains the PLP cofactor bound to Lys39, but instead of an aspartate it is an arginine residue (Arg224) which is located close to the pyridine ring, exhibiting a large N···N distance to the latter of 2.9 Å [93] as illustrated in Figure 14.33b. As arginine is more basic than pyridine, the latter does not seem to be protonated and the question arises as to which interaction then leads to the formation of the ketoamine tautomer.

In order to contribute to answering the open questions, the influence of hydrogen bonding to and protonation of the pyridine ring of PLP on its enolimine–ketoamine tautomerism has been studied by X-ray crystallography [96] and NMR [97] of solid model systems, and the influence of a polar environment by low-temperature liquid state NMR [98]. In these studies, correlations

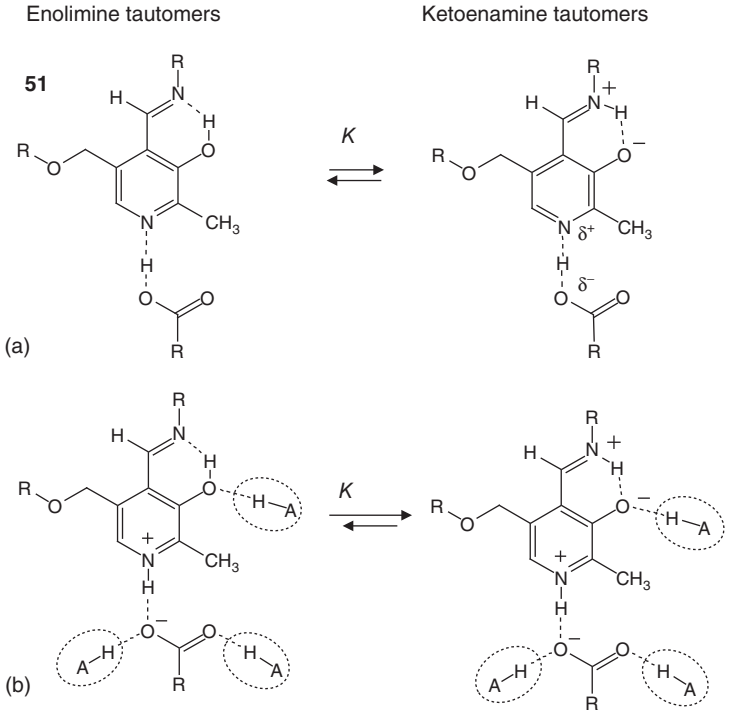

Figure 14.34 Tautomerism and protonation of model Schiff bases **51** according to [96–98].

between hydrogen bond geometries and ^{1}H and ^{15}N chemical shifts of PLP Schiff base models were derived. The equilibrium constants K of tautomerism were small in the absence of proton donors but increased when the pyridine ring formed hydrogen bonds with carboxylic acids. The larger their acidity the more H was displaced toward the pyridine nitrogen, and the more K was increased as illustrated schematically in Figure 14.34. But only when additional proton donors such as alcohols were added in polar organic solutions the ketoenamine tautomer was formed exclusively.

In subsequent NMR studies of aspartate aminotransferase and alanine racemase [94, 95] the NH and OH distances in Figure 14.33 marked in bold could be estimated from the NMR parameters, which confirmed that the pyridine ring is protonated in aspartate aminotransferase but not in alanine racemase. Unfortunately, the ^{15}N chemical shifts of the Schiff base nitrogens could not be measured, but PLP Schiff base model studies in poly-L-lysine [95] indicated that also hydrogen bond formation to the phenolic oxygen favors the ketoenamine tautomer as illustrated in the lower part of Figure 14.32. A similar effect was also found before in solution as was discussed in the previous section (Figure 14.30). Thus, it was proposed that O-protonation is operative in alanine racemase for the activation of PLP.

Moreover, it was found that the hydrogen bond geometries in alanine racemase indicate that PLP is embedded in a nonaqueous but polar environment exhibiting dielectric constant close to 30, and not in an aqueous environment. This finding is along the same line as discussed above in the case of HCA II.

Finally, the question of what happens when an aspartate carboxylate and a pyridine ring come close to each other in the active site of an enzyme was discussed [87]. As the active site resembles the organic wet polar environment and as the acid–base groups are no longer solvated by water molecules the free energy gain by taking up a proton from the water phase is substantial as it allows both residues to form a strong hydrogen bond. However, the location of the proton in this direct acid–base hydrogen bond is no longer governed by pK_a's but by the local electrostatics.

14.5 Conclusions

In the present account, examples for different kinds of tautomerizations have been presented as depicted in Figure 14.35. Traditionally, systems exhibiting intramolecular single or multiple proton transfers along intramolecular hydrogen bonds AHB (Figure 14.35a) are considered as tautomeric. Here, we propose that there can be any molecular link between the nuclei A and B, not just a series of

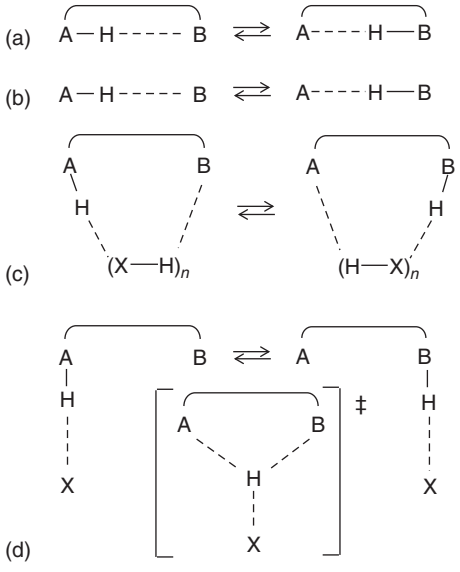

Figure 14.35 Main types of proton tautomerizations. (a) Intramolecular H transfer. (b) Intermolecular H transfer. (c) Proton tautomerization coupled to intermolecular proton transfer. (d) Intramolecular H-transfer proceeding via a coupled intermolecular H-transfer to a base and subsequent hydrogen bond switch.

conjugated single and double bonds or rings as proposed in the IUPAC definition of Eq. (14.1) [1]. Thus, electrical charges are omitted in Figure 14.35, which will appear when the molecular link constitutes an aliphatic chain. In addition, also a simple hydrogen bond may constitute such a molecular link. Therefore, intermolecular proton transfers in hydrogen-bonded acid–base complexes (Figure 14.35b) may also be regarded as tautomerizations. This is also justified in view of the similarities discussed above between intra- and intermolecular tautomerizations. We note that depending on the molecular symmetry, major changes of the hydrogen bond geometries can occur during the tautomerization.

Traditionally also systems are considered as tautomeric when a bifunctional catalyst takes up a proton at one atomic site and transfers another proton to any other site (Figure 14.35c). Another important mechanism, that is, when a catalyst X takes up a proton from a nuclear site A and carries it via a hydrogen bond switch to another nucleus has received little attention (Figure 14.35d).

When discussing molecular tautomerizations, one should keep in mind the hydrogen bond correlations depicted in Figure 14.1. Major hydrogen bond changes can occur; it will be a great difference if the tautomerization takes place along a hydrogen bond of medium strength or in a strong hydrogen bond.

It follows that there may be several elementary steps that constitute a tautomerization. But on the other hand, tautomerizations are coupled to a number of other phenomena, in particular hydrogen bond switches, molecular motions, and solvent reorganization. Even tautomerizations may constitute one of many elementary steps of complex molecular reactions, in particular of enzyme reactions. By using combinations of various spectroscopic and computational methods it will be interesting to extend the research area of tautomerism to more and more complex systems.

Acknowledgments

We thank all collaborators and colleagues who have contributed to the work described in this article. They are all mentioned in the references.

References

1. IUPAC (1997) *Compendium of Chemical Terminology (Gold Book)*, Version 2.3.3, 201402–24 (Compiled by McNaught, A.D. and Wilkinson, A. XML on–line corrected version created by Nic, M., Jirat, J., Kosata, B. updates compiled by Jenkins, A. ISBN 0–9678550–9–8), Blackwell Scientific Publications, Oxford, http://goldbook.iupac.org/T06252.html (accessed 28 November 2015).
2. Limbach, H.H. (2002) in *Encyclopedia of Nuclear Magnetic Resonance*, Advances in NMR, Supplementary, vol. **9** (eds D.M. Grant and R.K. Harris), John Wiley & Sons, Ltd, Chichester, pp. 520–531.
3. Limbach, H.H., Denisov, G.S., and Golubev, N.S. (2005) in *Isotope Effects in Chemistry and Biology*, Chapter 7 (eds

A. Kohen and H.H. Limbach), Taylor & Francis, Boca Raton, FL, pp. 193–230.
4. Limbach, H.H. (2007) in *Hydrogen Transfer Reactions*, Chapter 6 (eds J.T. Hynes, J. Klinman, H.H. Limbach, and R.L. Schowen), Wiley–VCH Verlag GmbH, Weinheim, pp. 135–221.
5. Limbach, H.H., Tolstoy, P.M., Pérez–Hernández, N., Guo, J., Shenderovich, I.G., and Denisov, G.S. (2009) OHO hydrogen bond geometries and NMR chemical shifts: from equilibrium structures to geometric H/D isotope effects with applications for water, protonated water and compressed ice. *Israel J. Chem.*, **49**, 199–216.
6. Pauling, L. (1947) Atomic radii and interatomic distances in metals. *J. Am. Chem. Soc.*, **69**, 542–553.
7. Steiner, T.J. (1998) Lengthening of the covalent X–H bond in heteronuclear hydrogen bonds quantified from organic and organometallic neutron crystal structures. *J. Phys. Chem. A*, **102**, 7041–7052.
8. Benedict, H., Limbach, H.H., Wehlan, M., Fehlhammer, W.P., Golubev, N.S., and Janoschek, R. (1998) Theoretical studies of primary and secondary geometric H/D isotope effects on low–barrier NHN–hydrogen bonds. *J. Am. Chem. Soc.*, **120**, 2939–2950.
9. Lorente, P., Shenderovich, I.G., Buntkowsky, G., Golubev, N.S., Denisov, G.S., and Limbach, H.H. (2001) $^{1}H/^{15}N$ NMR chemical shielding, dipolar $^{15}N,^{2}H$ coupling and hydrogen bond geometry correlations in a novel series of hydrogen bonded acid–base complexes of collidine with carboxylic acids. *Magn. Reson. Chem.*, **39**, S18–S29.
10. Limbach, H.H., Pietrzak, M., Benedict, H., Tolstoy, P.M., Golubev, N.S., and Denisov, G.S. (2004) Empirical corrections for quantum effects in geometric hydrogen bond correlations. *J. Mol. Struct.*, **706**, 115–119.
11. Ip, B.C.K., Shenderovich, I.G., Tolstoy, P.M., Frydel, J., Denisov, G.S., Buntkowsky, G., and Limbach, H.H. (2012) Geometric hydrogen bond H/D isotope effects and isotopic polymorphism of solid 4–Methylpyridine–Pentachlorophenol revealed by NMR: implications for the shapes of hydrogen–bonded protons in the solid and the liquid state. *J. Phys. Chem. A*, **116**, 11370–11387.
12. Benedict, H., Shenderovich, I.G., Malkina, O.L., Malkin, V.G., Denisov, G.S., Golubev, N.S., and Limbach, H.H. (2000) Nuclear scalar spin-spin couplings and geometries of hydrogen bonds. *J. Am. Chem. Soc.*, **122**, 1979–1988.
13. Shenderovich, I.G., Lesnichin, S.B., Tu, C., Silverman, D.N., Tolstoy, P.M., Denisov, G.S., and Limbach, H.H. (2015) NMR studies of active site properties of human carbonic anhydrase II using ^{15}N labeled 4-methylimidazole as a local probe and histidine hydrogen bond correlations. *Chem. Eur. J.*, **21**, 2915–2929.
14. Limbach, H.H., Schowen, K.B., and Schowen, R.L. (2010) Heavy atom motions and tunneling in hydrogen transfer reactions: the importance of the pre–tunneling state. *J. Phys. Org. Chem.*, **23**, 586–605.
15. Smirnov, S.N., Golubev, N.S., Denisov, G.S., Benedict, H., Schah-Mohammedi, P., and Limbach, H.H. (1996) Hydrogen/deuterium isotope effects on the NMR chemical shifts and geometries of intermolecular low-barrier hydrogen bonded complexes. *J. Am. Chem. Soc.*, **118**, 4094–4101.
16. Golubev, N.S., Denisov, G.S., Smirnov, S.N., Shchepkin, D.N., and Limbach, H.H. (1996) Evidence by NMR of temperature-dependent solvent electric field effects on proton transfer and hydrogen bond geometries. *Z. Phys. Chem.*, **196**, 73–84.
17. Perrin, C.L. and Lau, J.S. (2010) Are short, low-barrier hydrogen bonds unusually strong? *Acc. Chem. Res.*, **43**, 1550–1557.
18. Lopez del Amo, J.M., Langer, U., Torres, V., Buntkowsky, G., Vieth, H.M., Pérez-Torralba, M., Sanz, D., Claramunt, R.M., Elguero, J., and Limbach, H.H. (2008) NMR studies of ultrafast intramolecular proton tautomerism in crystalline and amorphous N, N′–Diphenyl–6–aminofulvene–1–aldimine: solid state, kinetic isotope and

tunnel effects. *J. Am. Chem. Soc.*, **130**, 8620–8632.

19. Braun, J., Hasenfratz, C., Schwesinger, R., and Limbach, H.H. (1994) Free acid porphyrin and its conjugated monoanion. *Angew. Chem. Int. Ed. Engl.*, **33**, 2215–2217.
20. Braun, J., Schwesinger, R., Williams, P.G., Morimoto, H., Wemmer, D.E., and Limbach, H.H. (1996) Kinetic H/D/T isotope and solid state effects on the tautomerism of the conjugated porphyrin monoanion. *J. Am. Chem. Soc.*, **118**, 11101–11110.
21. Braun, J., Schlabach, M., Wehrle, B., Köcher, M., Vogel, E., and Limbach, H.H. (1994) NMR study of the tautomerism of porphyrin including the kinetic HH/HD/DD isotope effects in the liquid and the solid state. *J. Am. Chem. Soc.*, **116**, 6593–6604.
22. Braun, J., Limbach, H.H., Williams, P.G., Morimoto, H., and Wemmer, D.E. (1996) Observation of kinetic tritium isotope effects by dynamic NMR. Example: the tautomerism of porphyrin. *J. Am. Chem. Soc.*, **118**, 7231–7232.
23. Schlabach, M., Rumpel, H., and Limbach, H.H. (1989) Investigation of the tautomerism of ^{15}N–labeled hydroporphyrins by dynamic NMR spectroscopy. *Angew. Chem. Int. Ed. Engl.*, **28**, 76–79.
24. Schlabach, M., Scherer, G., and Limbach, H.H. (1991) Kinetic HH/HD/DH/DD isotope effects on nondegenerate stepwise double proton transfer reactions. NMR study of the tautomerism of meso-tetraphenylchlorin. *J. Am. Chem. Soc.*, **113**, 3550–3558.
25. Wehrle, B. and Limbach, H.H. (1989) NMR study of environment modulated proton tautomerism in crystalline and amorphous phthalocyanine. *Chem. Phys.*, **136**, 223–247.
26. Hoelger, C.G., Wehrle, B., Benedict, H., and Limbach, H.H. (1994) High–resolution solid–state NMR relaxometry as a kinetic tool for the study of ultrafast proton transfers in crystalline powders. Example: dimethyldibenzotetraaza[14]annulene. *J. Phys. Chem.*, **98**, 843–851.
27. Langer, U., Latanowicz, L., Hoelger, C., Buntkowsky, G., Vieth, H.M., and Limbach, H.H. (2001) ^{15}N and ^{2}H NMR relaxation and kinetics of stepwise double proton and deuteron transfer in polycrystalline tetraaza[14]annulene. *Phys. Chem. Chem. Phys.*, **3**, 1446–1458.
28. Wehrle, B., Limbach, H.H., Köcher, M., Ermer, O., and Vogel, E. (1987) ^{15}N–CPMAS–NMR study of the problem of NH tautomerism in crystalline porphin and porphycene. *Angew. Chem. Int. Ed. Engl.*, **26**, 934–936.
29. Lopez del Amo, J.M., Langer, U., Torres, V., Pietrzak, M., Buntkowsky, G., Vieth, H.M., Shibl, M.F., Kühn, O., Broering, M., and Limbach, H.H. (2009) Isotope and phase effects on the proton tautomerism in polycrystalline porphycene revealed by NMR. *J. Phys. Chem. A*, **113**, 2193–2206.
30. Langer, U., Hoelger, C., Wehrle, B., Latanowicz, L., Vogel, E., and Limbach, H.H. (2000) A ^{15}N NMR study of proton localization and proton transfer thermodynamics and kinetics in polycrystalline porphycene. *J. Phys. Org. Chem.*, **13**, 23–34.
31. Pietrzak, M., Shibl, M.F., Broering, M., Kühn, O., and Limbach, H.H. (2007) ^{1}H/^{2}H NMR studies of geometric H/D isotope effects on the coupled hydrogen bonds in porphycene derivatives. *J. Am. Chem. Soc.*, **129**, 296–304.
32. Kyrychenko, A., Herbich, J., and Waluk, J. (2014) in *Tautomerism: Methods and Theories*, Chapter 3 (ed L. Antonov), Wiley-VCH Verlag GmbH, Weinheim, pp. 49–78.
33. Thoburn, J.D., Lüttke, W., Benedict, C., and Limbach, H.H. (1996) Indigodiimine: a highly fluxional molecule that tautomerizes via double proton transfers. *J. Am. Chem. Soc.*, **118**, 12459–12460.
34. Rumpel, H. and Limbach, H.H. (1989) NMR study of kinetic HH/HD/DD isotope, solvent, solid–state effects on double proton transfer in azophenine. *J. Am. Chem. Soc.*, **111**, 5429–5441.
35. Rumpel, H., Limbach, H.H., and Zachmann, G. (1989) Liquid– and solid–state infrared and near–infrared

study of the proton dynamics in azophenine. *J. Phys. Chem.*, **93**, 1812–1818.

36. Otting, G., Rumpel, H., Meschede, L., Scherer, G., and Limbach, H.H. (1986) Dynamic liquid state NMR and IR study of tautomerism and conformations of tetraphenyloxalamidine, a novel small intramolecular double hydrogen transfer system. *Ber. Bunsen Ges. Phys. Chem.*, **90**, 1122–1129.
37. Scherer, G. and Limbach, H.H. (1989) Observation of a stepwise double proton transfer in oxalamidine which involves matched kinetic HH/HD/DD isotope and solvent effects. *J. Am. Chem. Soc.*, **111**, 5946–5947.
38. Scherer, G. and Limbach, H.H. (1994) Dynamic NMR study of the tautomerism of bicyclic oxalamidines: kinetic HH/HD/DD isotope and solvent effects. *J. Am. Chem. Soc.*, **116**, 1230–1239.
39. Scherer, G. and Limbach, H.H. (1994) Proton and heavy atom motions during the stepwise proton tautomerism of various oxalamidines. A semiempirical PM3–MNDO study. *Croat. Chem. Acta*, **67**, 431–440.
40. Limbach, H.H. and Seiffert, W. (1974) Dynamic processes in systems with hydrogen bonds. I. ^{1}H–NMR spectroscopic study of the cis–trans equilibrium and the hydrogen bond association of N,N'–bis(pentadeuterophenyl)–1–amino–3–iminopropene in carbon disulfide. *Ber. Bunsen Ges. Phys. Chem.*, **78**, 532–537.
41. Limbach, H.H. and Seiffert, W. (1974) Dynamic processes in systems with hydrogen bonds. II. ^{1}H–NMR spectroscopic study of the direct and indirect intermolecular proton exchange of N,N–bis(pentadeuterophenyl)–1–amino–3–iminopropene in carbon disulfide. *Ber. Bunsen Ges. Phys. Chem.*, **78**, 641–647.
42. Xue, Q.A., Horsewill, A.J., Johnson, M.R., and Trommsdorff, H.P. (2004) Isotope effects associated with tunneling and double proton transfer in the hydrogen bonds of benzoic acid. *J. Chem. Phys.*, **120**, 11107–11119.
43. Lopez del Amo, J.M., Männle, F., Wawer, I., Buntkowsky, G., and Limbach, H.H. (2007) NMR studies of double proton transfer in hydrogen bonded cyclic N,N′–bisarylformamidine dimers: conformational control, kinetic HH/HD/DD isotope effects and tunneling. *Phys. Chem. Chem. Phys.*, **9**, 4498–4513.
44. Klein, O., Aguilar–Parrilla, F., Lopez del Amo, J.M., Jagerovic, N., Elguero, J., and Limbach, H.H. (2004) Dynamic NMR study of the mechanisms of double, triple and quadruple proton and deuteron transfer in cyclic hydrogen bonded solids of pyrazole derivatives. *J. Am. Chem. Soc.*, **126**, 11718–11732.
45. Foces–Foces, C., Echevarría, A., Jagerovic, N., Alkorta, I., Elguero, J., Langer, U., Klein, O., Minguet–Bonvehí, M., and Limbach, H.H. (2001) A Solid State NMR, X–ray diffraction and *Ab initio* computational study of hydrogen bond structure and dynamics of pyrazole–4–carboxylic acid chains. *J. Am. Chem. Soc.*, **123**, 7898–7906.
46. Torres, V., Lopez del Amo, J.M., Langer, U., Buntkowsky, G., Vieth, H.M., Elguero, J., and Limbach, H.H. (2012) Kinetics of coupled double proton and deuteron transfer in hydrogen–bonded ribbons of crystalline pyrazole–4–carboxylic acid. *Z. Phys. Chem.*, **226**, 1125–1147.
47. Limbach, H.H. and Seiffert, W. (1980) NMR spectroscopic study of cyclic proton exchange between acetic acid and methanol in tetrahydrofuran–d_8. *J. Am. Chem. Soc.*, **102**, 538–542.
48. Gerritzen, D. and Limbach, H.H. (1984) Kinetic isotope effects and tunneling in cyclic double and triple proton transfer between acetic acid and methanol in tetrahydrofuran studied by dynamic ^{1}H and ^{2}H NMR spectroscopy. *J. Am. Chem. Soc.*, **106**, 869–879.
49. Meschede, L., Gerritzen, D., and Limbach, H.H. (1988) Dynamic NMR study of the interference between cyclic proton exchange, selfassociation and hindered rotation of diphenylformamidine in tetrahydrofuran. *Ber. Bunsen Ges. Phys. Chem.*, **92**, 469–485.
50. Männle, F. and Limbach, H.H. (1996) Observation of an intramolecular base–catalyzed proton transfer in 1,3–Di–4–fluorophenyl–triazene.

Angew. Chem. Int. Ed. Engl., **35**, 441–442.

51. Limbach, H.H., Männle, F., Denisov, G.S., and Detering, C. (2005) Base catalyzed intramolecular single vs. intermolecular double proton transfer: a dynamic NMR study of 1,3–Di–(4–fluorophenyl)–triazene. *Chem. Phys.*, **319**, 69–92.
52. Meschede, L. and Limbach, H.H. (1991) Dynamic NMR study of kinetic HH/HD/DD isotope effects of double proton transfer in cyclic bis(p–fluorophenyl)formamidine dimers. *J. Phys. Chem.*, **95**, 10267–10280.
53. Toney, M.D. and Kirsch, J.F. (1993) Lysine 258 in aspartate aminotransferase: enforcer of the Circe effect for amino acid substrates and general-base catalyst for the 1,3-prototropic shift. *Biochemistry*, **32**, 1471–1479.
54. Wehrle, B., Zimmermann, H., and Limbach, H.H. (1988) A solid state ^{15}N CPMAS NMR study of dye tautomerism in glassy polystyrene: site dependence of double minimum potentials and their motional averaging. *J. Am. Chem. Soc.*, **110**, 7014–7024.
55. Avvaru, B.S., Kim, C.U., Sippel, K.H., Gruner, S.M., Agbandje–McKenna, M., Silverman, D.N., and McKenna, R. (2009) A short, strong hydrogen bond in the active site of human carbonic anhydrase II. *Biochemistry*, **49**, 249–251.
56. Maupin, C.M., McKenna, R., Silverman, D.N., and Voth, G.A. (2009) Elucidation of the proton transport mechanism in human carbonic anhydrase II. *J. Am. Chem. Soc.*, **131**, 7598–7608.
57. Shimahara, H., Yoshida, T., Shibata, Y., Shimizu, M., Kyogoku, Y., Sakiyama, F., Nakazawa, T., Tate, S., Ohki, S., Kato, T., Moriyama, H., Kishida, K., Tano, Y., Ohkubo, T., and Kobayashi, Y. (2007) Tautomerism of histidine 64 associated with proton transfer in catalysis of carbonic anhydrase. *J. Biol. Chem.*, **282**, 9646–9656.
58. Tolstoy, P.M., Koeppe, B., Denisov, G.S., and Limbach, H.H. (2009) Combined NMR/UV–Vis spectroscopy in the liquid state: study of the geometries of strong OHO hydrogen bonds of phenols with carboxylic acids. *Angew. Chem. Int. Ed. Engl.*, **48**, 5745–5747.
59. Pietrzak, M., Try, A., Andrioletti, B., Sessler, J., Anzenbacher, P., and Limbach, H.H. (2008) The largest $^{15}N..^{15}N$ coupling constant across an NHN-hydrogen bond. *Angew. Chem. Int. Ed. Engl.*, **47**, 1123–1126.
60. Pietrzak, M., Wehling, J.P., Kong, S., Tolstoy, P.M., Shenderovich, I.G., López, C., Claramunt, R.M., Elguero, J., Denisov, G.S., and Limbach, H.H. (2010) Symmetrization of cationic hydrogen bridges of protonated sponges induced by solvent and counteranion interactions as revealed by NMR spectroscopy. *Chem. Eur. J.*, **16**, 1679–1690.
61. Lloyd-Jones, G.C., Harvey, J.N., Hodgson, P., Murray, M., and Woodward, R.L. (2003) Scalar coupling between the ^{15}N centres in methylated 1,8-diaminonaphthalenes and 1,6-diazacyclodecane: to what extent is $^{2H}J_{NN}$ a reliable indicator of N-N distance? *Chem. Eur. J.*, **9**, 4523–4535.
62. Lesnichin, S.B., Tolstoy, P.M., Limbach, H.H., and Shenderovich, I.G. (2010) Counteranion-dependent intra- vs. intermolecular hydrogen bonding and proton transfer of 2,2′-bipyridinium in CDF_3/CDF_2Cl observed by low-temperature NMR. *Phys. Chem. Chem. Phys.*, **12**, 10373–10379.
63. Gurinov, A.A., Lesnichin, S.B., Limbach, H.H., and Shenderovich, I.G. (2014) How short is the strongest hydrogen bond in the proton-bound homodimers of pyridine derivatives? *J. Phys. Chem. A*, **118**, 10804–10812.
64. Melikova, S.M., Rutkowski, K.S., Gurinov, A.A., Denisov, G.S., Rospenk, M., and Shenderovich, I.G. (2012) FTIR study of the hydrogen bond symmetry in protonated homodimers of pyridine and collidine in solution. *J. Mol. Struct.*, **1018**, 39–44.
65. Yamaguchi, S., Kamikubo, H., Kurihara, K., Kuroki, R., Niimura, N., Shimizu, N., Yamazaki, Y., and Kataoka, M. (2009) Low-barrier hydrogen bond in photoactive yellow protein. *Proc. Natl. Acad. Sci. U.S.A.*, **106**, 440–444.

66. Koeppe, B., Tolstoy, P.M., and Limbach, H.H. (2011) Reaction pathways of proton transfer in hydrogen-bonded phenol-carboxylate complexes explored by combined UV-Vis and NMR spectroscopy. *J. Am. Chem. Soc.*, **133**, 7897–7908.
67. Koeppe, B., Guo, J., Tolstoy, P.M., Denisov, G.S., and Limbach, H.H. (2013) Solvent and H/D isotope effects on the proton transfer pathways in heteroconjugated hydrogen-bonded phenol-carboxylic acid anions observed by combined UV–Vis and NMR spectroscopy. *J. Am. Chem. Soc.*, **135**, 7553–7566.
68. Pylaeva, S., Allolio, C., Koeppe, B., Denisov, G.S., Limbach, H.H., Sebastiani, D., and Tolstoy, P.M. (2015) Proton transfer in a short hydrogen bond caused by solvation shell fluctuations: an ab initio MD and NMR/UV study of an (OHO)-bonded system. *Phys. Chem. Chem. Phys.*, **17**, 4634–4644.
69. Judson, C.M. and Kilpatrick, M. (1949) The effects of substituents on the dissociation constants of substituted phenols. I. Experimental measurements in aqueous solutions. *J. Am. Chem. Soc.*, **71**, 3110–3115.
70. Brown, H.D., McDaniel, D.H., and Häfliger, O. (1955) in *Determination of Organic Structures by Physical Methods*, Chapter 14 (eds E.A. Braude and F.C. Nachod), Academic Press, New York, pp. 567–662.
71. Tolstoy, P.M., Schah-Mohammedi, P., Smirnov, S.N., Golubev, N.S., Denisov, G.S., and Limbach, H.H. (2004) Characterization of fluxional hydrogen bonded complexes of acetic acid and acetate by NMR: geometries, isotope and solvent effects. *J. Am. Chem. Soc.*, **126**, 5621–5634.
72. Guo, J., Tolstoy, P.M., Koeppe, B., Golubev, N.S., Denisov, G.S., Smirnov, S.N., and Limbach, H.H. (2012) Hydrogen bond geometries and proton tautomerism of homo-conjugated anions of carboxylic acids studied via H/D isotope effects on ^{13}C NMR chemical shifts. *J. Phys. Chem. A*, **116**, 11180–11188.
73. Guo, J., Tolstoy, P.M., Koeppe, B., Denisov, G.S., and Limbach, H.H. (2011) NMR study of conformational exchange and geometries of intramolecular hydrogen bonds in monoanions of succinic acid and derivatives. *J. Phys. Chem. A*, **115**, 9828–9836.
74. Guo, J., Koeppe, B., Tolstoy, P.M., and Limbach, H.H. (2011) Trimethylglycine Complexes with Carboxylic Acids and HF: Solvation by Polar Aprotic Solvent. *Phys. Chem. Chem. Phys.*, **13**, 2335–2341.
75. Shenderovich, I.G., Tolstoy, P.M., Golubev, N.S., Smirnov, S.N., Denisov, G.S., and Limbach, H.H. (2003) Low-temperature NMR studies of the structure and dynamics of a novel series of acid-base complexes of HF with collidine exhibiting scalar couplings across hydrogen bonds. *J. Am. Chem. Soc.*, **125**, 11710–11720.
76. Golubev, N.S., Shenderovich, I.G., Smirnov, S.N., Denisov, G.S., and Limbach, H.H. (1999) Nuclear scalar spin-spin coupling reveals novel properties of low-barrier hydrogen bonds in a polar environment. *Chem. Eur. J.*, **5**, 492–497.
77. Shenderovich, I.G., Burtsev, A.P., Denisov, G.S., Golubev, N.S., and Limbach, H.H. (2001) Influence of the temperature-dependent dielectric constant on the H/D isotope effects on the NMR chemical shifts and the hydrogen bond geometry of the collidine-HF complex in $CDF_3/CDClF_2$ solution. *Magn. Reson. Chem.*, **39**, S91–S99.
78. Golubev, N.S., Smirnov, S.N., Gindin, V.A., Denisov, G.S., Benedict, H., and Limbach, H.H. (1994) Formation of charge relay chains between acetic acid and pyridine observed by low temperature NMR. *J. Am. Chem. Soc.*, **116**, 12055–12056.
79. Tolstoy, P.M., Smirnov, S.N., Shenderovich, I.G., Golubev, N.S., Denisov, G.S., and Limbach, H.H. (2004) NMR studies of solid state-solvent and H/D isotope effects on hydrogen bond geometries of 1:1 complexes of collidine with carboxylic acids. *J. Mol. Struct.*, **700**, 19–27.

80. Tolstoy, P.M., Guo, J., Koeppe, B., Golubev, N.S., Denisov, G.S., Smirnov, S.N., and Limbach, H.H. (2010) Geometries and tautomerism of OHN hydrogen bonds in polar solution probed by H/D isotope effects on ^{13}C NMR chemical shifts. *J. Phys. Chem. A*, **114**, 10775–10782.
81. Limbach, H.H., Pietrzak, M., Sharif, S., Tolstoy, P.M., Shenderovich, I.G., Smirnov, S.N., Golubev, N.S., and Denisov, G.S. (2004) NMR-parameters and geometries of OHN- and ODN hydrogen bonds of pyridine-acid complexes. *Chem. Eur. J.*, **10**, 5195–5204.
82. Rospenk, M., Sobczyk, L., Schah-Mohammedi, P., Limbach, H.H., Golubev, N.S., and Melikova, S.M. (2001) Dimerization and solvent assisted proton dislocation in the low-barrier hydrogen bond of a Mannich base. A low-temperature NMR study. *Magn. Reson. Chem.*, **39**, S81–S90.
83. Hansen, P.E., Rozwadowski, Z., and Dziembowska, T. (2009) NMR studies of hydroxy Schiff bases. *Curr. Org. Chem.*, **22**, 194–215.
84. Sharif, S., Denisov, G.S., Toney, M.D., and Limbach, H.H. (2006) NMR studies of solvent-assisted proton transfer in a biologically relevant Schiff base: towards a distinction of geometric and equilibrium H–bond isotope effects. *J. Am. Chem. Soc.*, **128**, 3375–3387.
85. Golubev, N.S., Smirnov, S.N., Tolstoy, P.M., Sharif, S., Toney, M.D., Denisov, G.S., and Limbach, H.H. (2007) Observation by NMR of the tautomerism of an intramolecular OHOHN-charge relay chain in a model Schiff base. *J. Mol. Struct.*, **844–845**, 319–327.
86. Toney, M.D. (ed) (2011) Pyridoxal phosphate enzymology. *Biochim. Biophys. Acta, Proteins Proteomics*, **1814**, 1405–1608.
87. Limbach, H.H., Chan-Huot, M., Sharif, S., Tolstoy, P.M., Shenderovich, I.G., Denisov, G.S., and Toney, M.D. (2011) Critical hydrogen bonds and protonation states of pyridoxal 5′-phosphate revealed by NMR. *Biochim. Biophys. Acta, Proteins Proteomics*, **1814**, 1426–1437.
88. Snell, E.E. and Jenkins, W.T. (1959) The mechanism of the transamination reaction. *J. Cell. Comp. Physiol.*, **54** (Supp. 1), 161–177.
89. Christen, P. and Metzler, D.E. (eds) (1985) *Transaminases*, 1st edn, John Wiley & Sons, Inc., New York. ISBN 0-471-08501-4.
90. Bach, R.D. and Canepa, C. (1997) Theoretical model for pyruvoyl-dependent enzymatic decarboxylation of α-amino acids. *J. Am. Chem. Soc.*, **119**, 11725–11733.
91. Toney, M.D. (2014) Aspartate aminotransferase: an old dog teaches new tricks. *Arch. Biochem. Biophys.*, **544**, 119–127.
92. Jager, J., Moser, M., Sauder, U., and Jansonius, J.N. (1994) Crystal structures of E. coli aspartate aminotransferase in two conformations. *J. Mol. Biol.*, **239**, 285–305.
93. Au, K., Ren, J., Walter, T.S., Harlos, K., Nettleship, J.E., Owens, R.J., Stuart, D.I., and Esnouf, R.M. (2008) Structures of an alanine racemase from Bacillus anthracis (BA0252) in the presence and absence of (R)-1-aminoethylphosphonic acid (L-Ala-P). *Acta Crystallorg.*, **F64**, 327–333.
94. Sharif, S., Fogle, E., Toney, M.D., Denisov, G.S., Shenderovich, I.G., Tolstoy, P.M., Chan Huot, M., Buntkowsky, G., and Limbach, H.H. (2007) NMR localization of protons in critical enzyme hydrogen bonds. *J. Am. Chem. Soc.*, **129**, 9558–9559.
95. Chan-Huot, M., Dos, A., Zander, R., Sharif, S., Tolstoy, P.M., Compton, S., Fogle, E., Toney, M.D., Shenderovich, I.G., Denisov, G.S., and Limbach, H.H. (2013) NMR studies of protonation and hydrogen bond states of internal aldimines of pyridoxal 5'-phosphate acid-base in alanine racemase, aspartate aminotransferase and poly-L-lysine. *J. Am. Chem. Soc.*, **135**, 18160–18175.
96. Sharif, S., Powell, D.R., Schagen, D., Steiner, T.M., Toney, M.D., Fogle, E., and Limbach, H.H. (2008) X-ray crystallographic structures of enamine and amine Schiff bases of pyridoxal and its 1:1 hydrogen bonded complexes with benzoic acid derivatives: evidence for

coupled inter- and intramolecular proton transfer. *Acta Crystallogr.*, **B62**, 480–487.

97. Sharif, S., Schagen, D., Toney, M.D., and Limbach, H.H. (2007) Coupling of functional hydrogen bonds in pyridoxal-5′-phosphate-enzyme model systems observed by solid state NMR spectroscopy. *J. Am. Chem. Soc.*, **129**, 4440–4455.

98. Sharif, S., Denisov, G.S., Toney, M.D., and Limbach, M.D. (2007) NMR studies of coupled low- and high-barrier hydrogen bonds in pyridoxal-5′-phosphate model systems in polar solution. *J. Am. Chem. Soc.*, **129**, 6313–6327.